M 2020

U.PORTO
FEUP FACULDADE DE ENGENHARIA
UNIVERSIDADE DO PORTO

GEOMETRIC OPTIMIZATION OF PROCESS UNITS BASED ON CFD TECHNIQUES

JOANA MANUEL RAMOS DE ALMEIDA
DISSERTAÇÃO DE MESTRADO APRESENTADA
À FACULDADE DE ENGENHARIA DA UNIVERSIDADE DO PORTO EM
ENGENHARIA QUÍMICA

Acknowledgment

The development of this project was only possible with the support of several people, who helped me over these months of work to achieve my goals and to complete another stage of my academic training. I leave a few words of deep and heartfelt thanks.

I would like to express my gratitude to my supervisors Prof. João Moreira Campos, and Dr. José Daniel Araújo for their guidance, help and patience.

I would also like to thank Prof. Manuel Alves, Prof. José Carlos Lopes and Dr. Ricardo Santos for introducing, and enticing in me a passion for Computational Fluid Dynamics.

I would like to express my deepest thanks to my parents, Manuel and Elisabete, who always provided me the best they could and knew, for their support and years of investing in me as a Person, as a Woman. Their endless love is invaluable to me.

To my Engineering cousins, Ivo Timóteo, Ivone Trigo and Marco Nicolau, a word of appreciation for guiding the way, and for their endless words of advice given over these five years.

I would like to thank the rest of my family for their undaunted and unconditional support.

And lastly, to my dear friends David Nascimento, Eunice Carmo, Pedro Martins, Pedro Ramos, Luís Castro, and Mariana Bessa for their companionship and words of encouragement throughout this journey that has been the writing of my dissertation.

Abstract

The design and optimization of process units is of uttermost relevance in Chemical Engineering. Thus, understanding and modelling the phenomena involved in such units are activities that gain a high importance. Computational fluid dynamics (CFD) presents itself as a remarkably reliable tool to perform these activities, since it is capable to describe the complexity and detail of several simultaneous phenomena, such as hydrodynamics of fluid flows, mass and energy transport and/or chemical reaction.

Based on the open-source CFD software OpenFOAM®, a set of simulations numerically replicating tracer experiments in single-phase flow of an incompressible Newtonian fluid were performed. These simulations encompassed the influence of operating conditions (inlet flow velocity) and geometric parameters. This influence was tested for a limited set of values that can be illustrative of several phenomena. On this thesis, the focus was placed on the quantifications of dispersive effects and pressure drop. Two sets of simulations were carried out, in systems containing solid structures (in 2D and 3D geometries) with ordered voids defining a certain porosity. Afterwards, geometrical optimization was performed in 2D structures with obstacles of selected topology.

The 2D simulations were based on geometries composed by obstacles of rectangular or ellipsoidal shape. The results obtained in these simulations led to the conclusion that the rectangular topology offered the best compromise between the level of mixture and a reasonable value of pressure drop. Regarding the 3D simulations, an inclined structure (with a double tilt of 45º) build upon the repetition of unitary cubic cells was addressed. It was observed that increasing the inlet velocity led to a progressive growth of the dispersion coefficients and pressure drop values. The results also suggested the presence of small stagnant volume in the structure, and as such, an estimation of the percentage of the stagnant volume was made. Regarding the illustrative optimization tests performed on the 2D domains filled with rectangles, these were successfully concluded and implied the variation of 2 and 4 geometrical parameters. As intended, it was possible to obtain geometric parameter values that define structures with improved mixing and/or minimizing pressure drop. Although the potential of the fully automatic optimization procedure (developed in-house) was demonstrated, the tests also allowed to identify some limitations that require some improvement.

Keywords: CFD, OpenFOAM®, geometry modelling, optimization, dispersion, pressure drop

Resumo

O projeto e a otimização de unidades processuais são de extrema relevância na Engenharia Química. Assim, compreender e modelar os fenómenos envolvidos em tais unidades são atividades que ganham grande importância. A dinâmica de fluidos computacional (CFD) apresenta-se como uma ferramenta notavelmente confiável para realizar essas atividades, uma vez que é capaz de descrever a complexidade e o detalhe de diversos fenómenos simultaneamente, como a hidrodinâmica dos escoamentos de fluidos, transporte de massa e energia e/ou reação química.

Com base no software OpenFOAM® de código aberto, foi realizado um conjunto de simulações que replicam numericamente experiências de tracer (marcador) em escoamento monofásico de um fluido Newtoniano incompressível. Essas simulações abrangeram a influência das condições operacionais (velocidade do fluxo de entrada) e parâmetros geométricos. Essa influência foi testada para um conjunto limitado de valores que podem ser ilustrativos de vários fenómenos. Nesta tese, o foco foi colocado nas quantificações dos efeitos dispersivos e da queda de pressão. Foram realizados dois conjuntos de simulações, em sistemas contendo estruturas sólidas (em geometrias 2D e 3D) com vazios ordenados definindo uma determinada porosidade. Posteriormente, a otimização geométrica foi realizada em estruturas 2D com obstáculos da topologia selecionada.

As simulações 2D foram baseadas em geometrias compostas por obstáculos de formato retangular ou elipsoidal. Os resultados obtidos nessas simulações permitiram concluir que a topologia retangular ofereceu o melhor compromisso entre o nível de mistura e um valor razoável de queda de pressão. Em relação às simulações 3D, foi abordada uma estrutura inclinada (com dupla inclinação de 45°) construída a partir da repetição de células cúbicas unitárias. Observou-se que o aumento da velocidade de entrada permitiu um crescimento progressivo dos coeficientes de dispersão e dos valores de queda de pressão. Os resultados também sugeriram a presença de volumes estagnados na estrutura e, como tal, foi feita uma estimativa da percentagem do volume estagnado. Quanto aos testes de otimização ilustrativos realizados nos domínios 2D preenchidos com retângulos, estes foram concluídos com sucesso e implicaram na variação de 2 e 4 parâmetros geométricos. Como pretendido, foi possível obter valores de parâmetros geométricos que definem estruturas com melhor mistura e/ou minimização da queda de pressão. Embora o potencial do procedimento de otimização totalmente automático (desenvolvido internamente) tenha sido demonstrado, os testes também permitiram identificar algumas limitações que requerem melhorias.

Palavras-chave: CFD, OpenFOAM®, modelação de geometria, otimização, dispersão, queda de pressão

Index

List of Figures

List of Tables

Notation and Glossary

Latin Characters

A	area	m^2
C	concentration	$kg \cdot m^{-3}$
$\bar{C}$	concentration of the outflowing central solution	$kg \cdot m^{-3}$
C_0	tracer concentration in the radial inlet injection zone	$kg \cdot m^{-3}$
Co	Courant number	
d_p	particle diameter	m
D	characteristic dimension	m
D_i	dispersion coefficient	$m^2 \cdot s^{-1}$
D_m	molecular diffusion coefficient	$m^2 \cdot s^{-1}$
D_T	thermal diffusivity	$m^2 \cdot s^{-1}$
K_1	constant of the linear term of the Ergun equation	
K_2	constant of the quadratic term of the Ergun equation	
L	length of the reactor	m
L_x	length of rectangular obstacle	m
L_y	width of the rectangular obstacle	m
p	pressure	Pa
Pe	Péclet number	
Q	volumetric flow rate	$m^3 \cdot s^{-1}$
r_1	semimajor axis of the ellipse	m
r_2	semimajor axis of the ellipse	m
R	radius of the bed	m
R_i	tracer injection radius	m
Re	Reynolds number	
S	source term	
t	time	s
t_r	residence time	s
T	temperature	K
w_i	weight of each i objective function term	
u_{int}	interstitial velocity	$m \cdot s^{-1}$
U	superficial velocity	$m \cdot s^{-1}$
V	volume	m^3
x, y, z	coordinates	m

Greek Characters

α_1	inclination angle 1	
α_2	inclination angle 2	
ε	porosity	
θ	reduced time	
λ_n	positive root of Bessel function of first kind	
μ	dynamic viscosity	Pa·s
ν	kinematic viscosity	$m^2 \cdot s^{-1}$
ρ	density	$kg \cdot m^{-3}$
τ	space time	s

Functions

$F(t)$	dimensionless concentration function	
F_{obj}	objective function	
$E(t)$	residence time distribution function	s^{-1}
$J_0(x)$	Bessel function of first kind of zero order	
$J_1(x)$	Bessel function of first kind of first order	

Indexes

A	area
ax	axial
b	bypass
C	concentration
f	fluid
in	inlet
m	molecular
out	outlet
p	pressure
r	radial
s	surface
$stag$	stagnant
T	temperature

List of Acronyms

2D	Two Dimensional
3D	Three Dimensional
CEFT	Transport Phenomena Research Center
CFD	Computational Fluid Dynamics
CFL	Courant-Friedrich-Lewy
CPU	Central Process Unit
FEUP	Faculty of Engineering of the University of Porto
GPU	Graphics Processing Unit
LES	Large-Eddy Simulation (model)
OpenFOAM	Open source Field Operation And Manipulation
RAS	Reynolds-Averaged Stress (model)
RTD	Residence Time Distribution
STL	STereoLithography (file)

1 Introduction

1.1 Framing and Presentation of the Work

The current project was developed within the course of the dissertation for the Master's degree in Chemical Engineering. It was carried out in an academic environment at the Transport Phenomena Research Center (CEFT).

Nowadays, the chemical industry is still responsible for a very significant footprint in terms of energy consumption and waste generation. Thus, the modelling, design and optimization of the involved process units are crucial for their profitability and environmental impact.

The expression "design and optimization of a process unit" probably flashes a picture of an experimental apparatus in a Chemical Engineer's mind. This is quite normal considering it was not until the early 1980s that Computational Fluid Dynamics (CFD) became widely available. Currently, however, it is recognized as a valid and competitive tool to study, test and optimize systems involving fluid flows. But, "What is CFD exactly?" some might ask. CFD is a tool that performs simulations to describe with detail the hydrodynamics of fluid flows. The simulations may encompass the interactions of the fluid(s) in question with the surrounding surfaces, and phenomena such as mixing, heat and mass transfer and chemical reaction. These phenomena happen to be the core of the majority of the processes in Chemical Engineering and are deeply dependent on the operating conditions and geometric parameters of the process units. Hence, it is crucial that advanced computational methods are able to predict them with a good level of precision. Furthermore, with the booming of manufacturing technologies like 3D printing, besides a highly efficient utilization of energy and resources (almost zero solid residual waste), it is also allowed full freedom in an object geometrical design. Although this aspect can be decisive to change the way several types of process units are designed, it implies that simulation and optimization tools must be adapted/improved to follow and support the referred change.

The main objective of this project is to demonstrate the potential impact of the application of CFD in simulation and geometrical optimization. For this purpose, it was simulated and characterized the single-phase incompressible flow of a Newtonian fluid with simultaneous mass and/or heat transport through bi- and tridimensional porous structures through CFD techniques. Additionally, it was inspected the level of influence of different operating conditions (flow velocity) and geometric parameters on the hydrodynamics of the studied systems. Lastly, it was introduced an innovative and fully automatic optimization methodology, based on geometric parameters and a pre-defined objective function that maximizes mixing and the surface area, and minimizes the pressure drop.

For the CFD simulations, it was used an open source CFD software, OpenFOAM®, together with a pre-processor for the geometry modeling, Blender®, and a post-processor, ParaView®. For the optimization tests, the referred tools were coupled with the Nomad® optimizer.

The main physical results that were expected to be obtained are the temporal evolution of the variables fields (velocity, pressure, concentration, and temperature) and quantification of the axial dispersion, radial dispersion and pressure drop, and their dependence to operating conditions and geometrical parameters.

It is worth noting that the initial work plan included an experimental/validation part and a deeper optimization study with specific applications. Due to the pandemic period we are facing, this project was re-oriented towards an illustrative perspective of the potential of the tools involved. This potential can be used in a wide range of applications regarding the design and optimization of process units, from reactors to heat exchangers and adsorption columns. Nonetheless, the modeled geometries can be transposed to the physical world by reproducing them with 3D printing.

1.2 Presentation of the laboratory

CEFT, which in Portuguese stands for Centro de Estudos de Fenómenos de Transporte, is a research unit integrated into the Chemical and Mechanical Engineering Departments of the Faculty of Engineering of University of Porto (FEUP).

CEFT is focused on the sub-domain of transport phenomena (heat, mass, and momentum) bridging the main areas of Chemical and Mechanical engineering. This research unit was founded in 1996 by four teachers at FEUP, and has since grown steadily, into a medium-sized unit that potentiates independent research and enhances creativity.

CEFT dedication lies essentially in fundamental research where it has reached a significant success and built excellent quality scientific knowledge, often branching into practical applications.

The research carried out at CEFT is structured in two main topics:

- ENERGY - With emphasis on cleaner fuels, such as natural gas and biomass, as well as issues related to the carbon problem, and the hydrogen economy. For these issues, optimization and development of fuel cell technology and systems for hydrogen production and storage are being developed.
- FLUIDS - Addresses several sub-topics that are related and interact within each other: complex fluids, multiphase flows, intelligent fluids and biofluids. This approach is supported by the high knowledge of researchers from the group, both in appropriate experimental techniques and in advanced computational methods (particularly CFD).

1.3 Contribution of the author to the work

First and foremost, it is deeply important to note that for the execution of this thesis, I had to learn and understand in some depth the functioning of the used software (namely OpenFOAM®, Blender® and ParaView®). This involved learning two new code languages (C++ and Python™), which with all adding up implies a substantial learning curve. Therefore, a considerable amount of time in the technical execution of this dissertation was dedicated to this aspect. However, since we are talking about free-to-use tools, which are attractive from a company point of view, the acquisition of this type of knowledge may be of great value in the future in case I intend to enter the area of CFD; I am now prepared to generate a mesh for an intended case, set up the simulation case, and post-process the given results.

Relatively to the contributions on a scientific level, I adapted and improved geometry generation scripts in Blender®, I implemented a solver in OpenFOAM® to fit with the desired mathematical model, and I adjusted an optimization process with the various software involved. The most relevant output is that the optimization process is now much better prepared to be applied to different systems.

1.4 Organization of the thesis

This dissertation is divided into the following chapters:

In the Context and State of Art, a more detailed overview of what CFD is, its applicability in Chemical Engineering, and which software packages can be used is given. Afterwards, it is provided a summary of how the chosen CFD software works and the mathematical model that was implemented. An outline of specific studied features (dispersion and pressure drop) is given as well as a brief description of tracer tests and theoretical principles involved.

Materials and Methods is divided into pre-processing, setting up the simulation case, running the simulation, post-processing, and optimization approach, which is the complete methodology followed to obtain results.

The chapter Results and Discussion presents the relevant data extracted from the simulations and optimization tests performed, and an analytical discussion on whether the results obtained go against what would be expected.

Conclusion, where the main conclusions drawn from the project are summarized.

Assessment of the work done, where the work developed and the obstacles encountered are evaluated, suggesting future work and developments.

2 Context and State of the Art

2.1 Computational Fluid Dynamics

Since the dawn of civilization, mankind has always had a keen interest and fascination over fluids. From the flow of water in rivers, the flow of the wind in our atmosphere, the turmoil of the oceans, to the very down blood that flows in our bodies. For years, these and other kinds of flows (single and multiphase) were analysed solely through means of experimental studies and empirical correlations, until Computational Fluid Dynamics (CFD) came along.

CFD was developed from the combination of synergies between fluid mechanics, mathematics, and computer science. This computational tool is able to simulate the hydrodynamics of an entire flow field, including the interactions of the fluid(s) in question (liquid and/or gas) with the surrounding surfaces, together with other coupled phenomena such as heat and mass transfer and chemical reactions. In order to perform these simulations, it is necessary to know and define the geometry of the system and to establish adequate boundary conditions. So, the first step of a CFD simulation consists in the construction of the geometrical domain and splitting it into smaller elements (mesh generation). The number and size of the elements are highly dependent on the phenomena involved and the level of detail and accuracy to achieve.

The physics and chemistry should also be identified and modelled by a proper set of governing equations. The set of equations may include standard conservation of momentum, mass and energy, or express more complex features such as turbulence modelling, multiphase flow, phase equilibrium, non-Newtonian fluid behaviour and reaction kinetics. Depending on the goals to achieve, it can be taken a steady-state or an unsteady state approach – the latter option implies that some initial conditions must be prescribed. The governing equations are discretized into algebraic counterparts within the space and/or time domain and, afterwards, solved iteratively using computer algorithms embedded within the CFD software. A set of predicted discrete numbers/distributions is obtained for each variable of interest at the end of this process, i.e., the numerical solution. The numerical solution can be viewed graphically in colour plots of variable vectors, contours, lines of constant flow field properties and *x*-*y* plots.

CFD is an extremely flexible tool that can simulate almost all imaginable flows and as such it has a breadth of applications that spawns from aerodynamics, rheology, and turbomachinery to meteorology, combustion engines and electronics. To give a recent and notorious example of a practical application, due to the current pandemic caused by covid-19, scientists resorted to CFD simulations to determine and quantify the special evolution of aerosols and small droplets released while coughing, speaking, and breathing, in order to assess the risk of transmission of covid-19 in various public spaces (Vuorinen et all, 2020).

Although CFD is a powerful tool, it requires the complementarity of experimental techniques to validate models and numerical methods and determine their accuracy. In addition, if available, predictions made by empirical correlations may also be compared with corresponding simulation results to assess and confirm their quality. Once this validation is complete, it is less expensive to replicate experiments with CFD simulations than conducting physical ones. This is precisely the aspect where it lays the main advantage of CFD.

Physical experiments are run at the expense of materials that once the experiment is over, normally, are not reusable and go to waste. Additionally, physical testing can be time-consuming and more prone to failures, which add up to the final cost. CFD simulations, however, may require an initial investment of computer hardware (specifically, a powerful CPU or GPU) and sometimes of software (commercial licenses), but in the long run, it is expected to be less costly. On top of this, the sustainability character of a CFD approach is fully in-line with these arising concerns in the modern industry. Furthermore, physical experiments can be a hurdle, having sometimes to be performed at very harsh conditions such as extreme temperatures, pressures, flow velocities and can only be materialized in special/expensive equipment or on unwieldly devices. On the other hand, CFD simulations depend exclusively on computer software, which can be transported or even be accessed remotely. As aforementioned, it should be highlighted that CFD does not substitute physical experiments, but rather synergistically complements it, providing useful insights and details that were once out of reach through experimental and/or empirical approaches.

2.1.1 CFD in Chemical Engineering

The work of a Chemical Engineer is often to develop and design unit processes, such as reactors, heat exchangers, distillation columns, and storage tanks. Not only that, but also a Chemical Engineer has to deal with its internal flows, i.e., the flows confined by solid surfaces. Additionally, the pipes that connect the installation also have to be equated and designed (Campos, 2013). Even after the installation is set up, the need for optimization of the process units maintains, whose objectives vary according to the needs and limitations of each system. Some common examples of this type of objectives are to improve thermal efficiency, to decrease pressure drop, increase productivity and/or selectivity, decrease the amount required of reactants/catalysts, etc. Thus, being able to model and simulate the flow coupled with other relevant phenomena (such as mass and heat transfer and/or reaction) in process units in a manner that helps to maximize the desired product(s) is of extreme value for Chemical Engineers. A subset of illustrative examples of Chemical Engineering areas where CFD can be used is given below.

Many Chemical Engineers work in the polymers industry, e.g. foaming polyurethane flow through a closed cabinet can be simulated through CFD tools (Baser and Khakhar, 1994). Water treatment is another important Chemical Engineering subject, where is essentially involved water flow through chemical,

physical, or/and biological treatments, and whose optimization can benefit from CFD. Other prominent Chemical Engineering field is the oil refinery, where combustion takes place and the flow of oil and gas needs to be studied for the design of pipelines and equipment, and requires constant optimization, both of which can be made resorting to CFD tools (Bayat et all, 2012). Distillation, in its broad sense, is a matter for Chemical Engineers, from distillation of fermented products to create distilled beverages with high alcohol content (Rao and Barik, 2012), to desalination (Sousa et all, 2014), and even Cryogenic Distillation, which leads to the separation of air into its components (oxygen, nitrogen, and argon) (Hajilary and Rezakazemi, 2018). All of which, can take advantage of simulation tools. Batteries, which generate electrical energy (voltage) through chemical reactions, can also be simulated by CFD software to study and optimize these systems and avoid experimental waste of valuable components (metals and electrolytes) (Pinto, Oliveira, and Falcão, 2018). Needless to say, in any research facility or industry where there is a chemical reaction, there is a Chemical Engineer. Predicting the dynamics of fluids inside of reactor units, to optimize the desired performance and obtain reliable operating conditions, is of uttermost importance and can be well captured through Computational Fluid Dynamics simulation (Ansoni and Seleghim, 2016).

2.1.2 Licensed vs. Open-source Software

To increase the cost-effectiveness nature of CFD simulations, engineers can resort to open source CFD software packages, which are usually freely licensed. Open source packages are very versatile in terms of modelling since it is allowed an almost free implementation of different simultaneous features in the codes. This becomes particularly relevant as the complexity of the systems increase. Also, the user can have a wide and more effective control over the entire simulation procedure. However, the open source options also offer some drawbacks in comparison with commercial licenses. These options are less user-friendly at a basic level and, if it is desired to add more functionalities through coding, it requires more knowledgeable and skilled users. Since commercial licenses are paid, with annual licenses in the range of thousands of euros, user-support and documentation are prominent features while for open-source can be rather limited. Commercial software packages are, however, more intuitive, well developed and include a large number of tools and functionalities for pre- and post-processing without the need for coding. Open source packages may require additional software, as pre- and post-processors are often not included.

A subset of CFD software is listed below.

Regarding freely licensed options, OpenFOAM® is the leading open source software, developed by OpenFOAM Foundation. The code is programmed in C++ language and it runs on Linux, macOS and Windows 10 operating systems. This package is known for being a well-rounded software that can simulate turbulence, thermophysics, transport modeling, heat and mass transfer, electromagnetic modeling, reacting flows, both incompressible and compressible fluid flows, multiphase flows, combustion, amongst others. The OpenFOAM® community is increasingly growing, with users ranging from across all sorts of

industries, some being notably relevant in the Chemical Engineering field. Based on the aforementioned aspects, OpenFOAM® was the CFD software used in the present thesis. SU2® is another example of an open source software, written in C++ and Python, and developed by Stanford University and is an acronym for Stanford University Unstructured. Its key feature is the fact that comprehensive documentation and tutorials are provided upon installation, making it an accessible software to learn. It was developed with the focus on aerodynamic optimization, but is extensible to other fields such as electrodynamics, reacting flows, elasticity, just to name a few. Advanced Simulation Library® (ASL) is an open source platform developed by Avtech Scientific. It is C++ based and runs on Windows, Linux, Mac OS X, and Unix. It provides a range of features that can simulate complex fluid flows involving chemical reactions, turbulence, heat transfer, solid mechanics, and elasticity.

As for commercial licenses, Fluent® is the leading paid licensed CFD software. It is notoriously known for having a user-friendly interface and a faster learning curve. It was developed by ANSYS® and has modeling capabilities that include turbulence, multiphase flows, heat and mass transfer, combustion, and multiphysics. COMSOL Multiphysics® comes in a close second as the leading paid software that can be used for a broad range of multiphysics problems. It is notable for solving chemical, electrical, mechanical, fluid, and even acoustics applications, and comes with a set of geometry tools that facilitates parametric studies and can support both linear and nonlinear equation systems. Engineers and scientists can resort to COMSOL Multiphysics® to model designs as part of the product development process. Autodesk® CFD is a paid licensed software whose top feature is thermal simulation, being able to solve all modes of heat transfer, including solid-to-solid and solid-to-fluid transfers. Its main application is solving steady-state, single-phase, non-reacting flow systems and has a focus on the ease of use. Finally, there is SimScale®, a paid software that operates in an innovative way, as both the software and its infrastructure reside entirely in the cloud. It means that working with it has a zero-size hardware footprint, so, simulations can be run from practically any device. Hence, unlike the previously mentioned software packages, it requires no investment in powerful servers while offering a computer power that could be otherwise unaffordable. Its major drawback is the cost, as the annual subscription can be pricey.

2.2 OpenFoam® case structure

As previously mentioned, OpenFOAM® (version 4.1) was the CFD software chosen for this dissertation. Every OpenFOAM® simulation case must be set up in a predestined manner which contains a minimum of three directories. These directories are “0”, “constant” and “system” that contain subfolders and files to establish the conditions in which the simulation will take place. The typical structure of an OpenFOAM® simulation case can be seen in Figure 2.1.

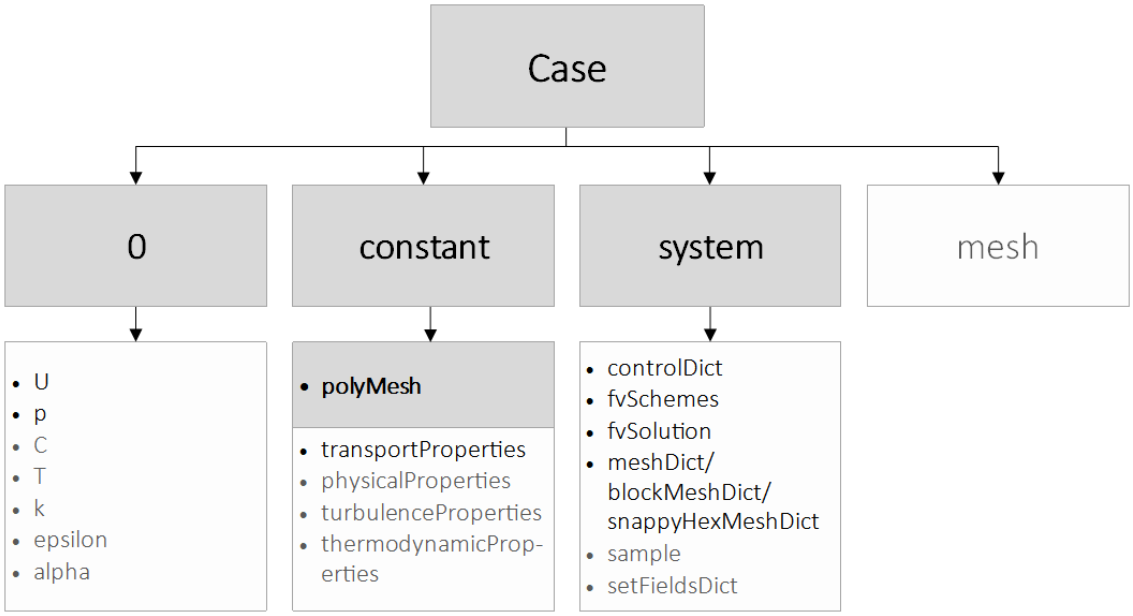

Figure 2.1-Case structure in OpenFOAM®.

2.2.1 Folder "0"

This folder contains files with the initial and boundary conditions of the used variables. For laminar incompressible isothermal systems (and single phase), the only files needed regard the velocity (vector variable *U*) and pressure (scalar variable *p*). When there is transport of one or more properties, whether it being mass or heat, then other variable/s must be added as well, e.g. concentration (scalar variable *C*) or/and temperature (scalar variable *T*). If the flow is turbulent, then additional files should be included concerning variables of the corresponding model, e.g. *k*, and *epsilon*, which correspond to the turbulent kinetic energy and the turbulent dissipation coefficient, respectively. Likewise, if the flow is multiphase then the file *alpha*, corresponding to the phase fraction field, must also be added. Three types of entries are mandatory in for each variable file: the primary dimensions of the variables in SI units (e.g. $[kg \cdot m^{-1} \cdot s^{-2}]$ for pressure), the initial condition of the internal field (e.g. a system that is initially stagnant should have zero velocity in all coordinates) and the boundary field (e.g. inlet, outlet and wall conditions).

2.2.2 Folder "constant"

This folder contains the files that define the properties of the system to simulate. Depending on the chosen solver, that is the mathematical model and the conditions intended to simulate, different files require specification by the user. For example, in solvers for incompressible laminar flow, the file *transportProperties* includes the value of the kinematic viscosity ν. Also in *transportProperties*, if the flow is multiphasic then the file defines the phases and the corresponding transport model for each, as well as the surface tension between the phases. For compressible solvers, a *thermodynamicsProperties* file is required, where an equation of state is set along with a specific heat value and Prandtl number (a dimensionless number defined as the ratio of momentum diffusivity to thermal diffusivity). In the case of mass or/and energy transport, normally it is created a *physicalProperties* file where the diffusivity

coefficients are set, both its dimension and magnitude. The information about the type of turbulence model (when applied) is introduced in *turbulenceProperties* where either laminar, RAS or LES models can be chosen.

Another important part of the "constant" directory is the "polyMesh" subfolder that contains the information about the mathematical mesh. This subfolder is initially empty but, when the mesh is generated, the corresponding files describing the mesh will appear (*points*, *faces*, *owner*, *neighbor,* and *boundary*).

2.2.3 Folder "system"

This folder contains the specifications for the numerical methods to use during the simulation. In *controlDict* file, the frequency of solution file outputs, run time, number of time steps and Courant number are assigned. The Courant-Friedrichs-Lewy (CFL) number is a mandatory and crucial condition for convergence in transient state simulation processes. In order to achieve temporal accuracy and numerical stability, a dimensionless Courant number, Co, less than unity is frequently appropriate. The Courant number (Courant et all, 1928) is normally defined for one cell as:

$$\mathrm{Co} = \frac{\Delta t |U|}{\Delta x} \tag{2.1}$$

where Δt is the time step, U the velocity magnitude of the fluid in the x-direction and Δx a characteristic size of the mesh elements.

Another important file is the *fvSchemes*. In this file, the user defines the numerical discretisation schemes to apply during the simulation. In the *fvSolution* file, the necessary parameters for the chosen numerical schemes are assigned, as well as tolerances, maximum number of iterations (depending on the solver) and convergence criteria. Finally, there is always a *meshDict* type of file, where the information to generate the mesh is given, with its name varying depending on the mesh generator used. Some notorious examples include *blockMeshDict* for BlockMesh, *meshDict* for CF-MESH+® and *snappyHexMeshDict* for SnappyHexMesh. Additional (optional) files can be added such as *sample*, which is a post-processing tool, and *setFieldsDict*, which is used for patching (assigning an amount to a region) in the simulation, amongst others.

2.3 Governing equations (Model)

The starting point of any numerical simulation is the governing equations that define the CFD model to solve by the software.

The set of equations that describe a viscous flow are known as the Navier-Stokes equations. These equations embody the principles of conservation of momentum (Newton's 2nd law), mass, and/or energy (1st law of thermodynamics). They arise from applying Newton's second law to fluid motion, coupled with the assumption that the stress in the fluid is the sum of a pressure term and a diffusing viscous term (proportional to the gradient of velocity). Thus, the momentum equation for a laminar incompressible flow, i.e. a fluid whose mass and volume does not change under pressure and, as such, density is constant over time for the volume element, is given by:

$$\underbrace{\frac{\partial \boldsymbol{U}}{\partial t}}_{\text{time derivative}} + \underbrace{\nabla \cdot (\boldsymbol{U}\boldsymbol{U})}_{\text{convection term}} = \underbrace{-\nabla p}_{\text{pressure term}} + \underbrace{\nu \Delta \boldsymbol{U}}_{\text{diffusion term}} \tag{2.2}$$

where $\boldsymbol{U}$ denotes the velocity vector, p is the kinematic pressure (p/ρ) and ν is the kinematic viscosity (μ/ρ). The solution of the equation is the velocity vector field - for every point in a fluid, at any moment, it gives a vector whose magnitude and direction are those of the velocity of the fluid.

The incompressible Navier-Stokes continuity equation is:

$$\nabla \cdot \boldsymbol{U} = 0 \tag{2.3}$$

For both mass and energy quantities, the transport equation is similar and described as follows. The mass equation is the convection-diffusion equation that comes from Fick's second law:

$$\underbrace{\frac{\partial C}{\partial t}}_{\text{time derivative}} + \underbrace{\nabla \cdot (\boldsymbol{U}\boldsymbol{C})}_{\text{convection term}} = \underbrace{D_m \Delta C}_{\text{diffusion term}} + \underbrace{S_C(C)}_{\text{source term}} \tag{2.4}$$

And the heat equation is given by:

$$\underbrace{\frac{\partial T}{\partial t}}_{\text{time derivative}} + \underbrace{\nabla \cdot (\boldsymbol{U}T)}_{\text{convection term}} = \underbrace{D_T \Delta T}_{\text{diffusion term}} + \underbrace{S_T(T)}_{\text{source term}} \tag{2.5}$$

The terms from left to right represent the rate of change per unit volume, the convection rate, the rate of transport due to diffusion, and the rate of production/destruction. For the case of mass, the source term S_C accounts for the existence of a reaction, i.e., if there is no reaction and/or describing the transport of an inert then S_C = 0, whilst if there is a reaction the source term is equal to the kinetics equation, which depends on the reaction rate constants and order of the reaction. Similarly, heat can also be generated/consumed, which influences the thermal source term, S_T.

It should be noted that, as aforementioned, what CFD codes do is a discretisation, i.e., it converts the continuum solution of the governing equations into discrete quantities.

2.4 Main hydrodynamic characteristics in fixed bed process units

The hydrodynamic characterization of a flow is a topic of central importance in Chemical Engineering. CFD simulations can be used to provide insights into the flow patterns, local variations of flow variables and their dependence on different operating and geometrical parameters.

First and foremost, the Reynolds number, Re, which measures the ratio of inertial forces to viscous forces acting on a fluid element, is an essential dimensionless group to characterize flow patterns:

$$\mathrm{Re} = \frac{\text{Inertial forces}}{\text{Viscous forces}} = \frac{\rho u D}{\mu} \tag{2.6}$$

At low Reynolds numbers, when the viscous forces are dominant, the flow is said to be laminar, characterized by smooth, constant fluid motion. However, if the flow is chaotic and produces vortices and other flow instabilities, then it is turbulent, having a high Reynolds number, which means the inertial forces are dominant.

Axial and radial dispersion are important features that affect the mass transfer performance of a process unit. As such, different operating conditions (flow velocity) and geometric parameters influence the mixing. In the same way, these aspects influence pressure drop, which ideally should be minimized. A small description about the main theoretical principles involved is given below.

2.4.1 Axial and Radial Dispersion

Dispersion is the process of "spreading" (or distributing) a given substance in a given medium. Its coefficient, D, quantifies this distribution in an expeditious way, where a higher coefficient means a faster distribution, and naturally, a lower coefficient represents a slower distribution. Dispersion is a phenomenon regulated by the hydrodynamics of the system and can be estimated either from correlations in the literature, experimental tests or CFD simulations.

One of the dimensionless terms used to describe the relation between the rate of dispersion and the rate of convection is Péclet number, Pe:

$$\mathrm{Pe} = \frac{\tau_{\text{dispersion}}}{\tau_{\text{convection}}} = \frac{L^2/D}{V/Q} = \frac{L^2/D}{LA/uA} = \frac{uL}{D} \tag{2.7}$$

where u denotes the flow velocity, L is the characteristic length of the given medium, and D is the dispersion coefficient.

When Pe tends to 0 then there is perfect mixing, i.e., a large amount of dispersion, and the transport by convection is insignificant. The flow can be approximated to one of a continuous stirred vessel. Conversely, if Pe tends to infinite, then convection is dominant and there is a small amount of dispersion. The flow can be approximated to a plug flow system (Levenspiel, 1972).

In addition to the molecules diffusing relative to the average fluid velocity by molecular diffusion (Fick's law), whose coefficient is mass diffusivity, D_m, they can also move between streamlines in both axial and radial directions. Two other types of dispersion coefficients can then be defined: axial (D_{ax}) and radial (D_r). Hence, depending on the dispersion coefficient used, three Péclet numbers can be defined: Pe_m, Pe_{ax}, and Pe_r respectively.

The dispersion coefficients are generally measured in absence of reaction, since it is been observed that its values have direct dependence with mass transfer. A possible technique used to estimate both axial and radial dispersion consists of replicating the continuous feed of a tracer concentration in the inlet with CFD simulation. The numerical results of the tracer concentration field, and more specifically, the distribution of the tracer either throughout the structure in the z-direction (for D_{ax}) or outside a given central zone (D_r) can give estimates about the effect of the dispersion coefficients.

2.4.2 Pressure Drop

A fluid flowing through obstacles that promote flow path changes (such as a porous bed) exerts a force on the surfaces, whose components, normal and tangential, result from the integration of pressure and shear stress. The mechanical energy spent by the fluid when applying this force translates into a loss of energy from the flow of the fluid (i.e. loss of pressure). The pressure drop between two points, with fluid between them, can be defined as the pressure difference between the given points, due to pressure losses caused by the frictional forces on the flow.

Thus, the pressure drop depends on the porosity of the system, ε, which is determined by the fraction of the volume of voids over the total volume. From this premise, the Ergun equation is one of the most used to express pressure drop of fluids across fixed beds (Ergun, 1952):

$$\frac{(-\Delta p)}{L} = K_1 \frac{(1-\varepsilon)^2}{\varepsilon^3} \mu \frac{U}{d_p^2} + K_2 \frac{(1-\varepsilon)}{\varepsilon^3} \rho \frac{U^2}{d_p} \tag{2.8}$$

where $(-\Delta p)$ denotes the pressure drop, d_p the diameter of the particles, and K_1 and K_2 are constants. The constants are normally obtained by experiments, and typically is used K_1 = 150 and K_2 = 1.75.

The previous equation can be rewritten as a function of fluid Reynolds number:

$$\frac{(-\Delta p)}{L} = 150 \frac{(1-\varepsilon)}{\varepsilon^3} \rho \frac{U^2}{\mathrm{d}_p} \frac{1}{Re_f} + 1.75 \frac{1}{\varepsilon^3} \frac{\rho^2}{\mu} U^3 \frac{1}{Re_f} \tag{2.9}$$

Therefore, changing the geometry and size of the structures used in the beds will adjust the porosity, and implicitly the pressure drop. By analyzing the Ergun equation, it is easy to see that a low porosity of the bed will involve a greater pressure drop, something that goes against what normally is intended in the design of process units.

The traditional methods of measuring pressure drop involve *in-situ* determination at the entrance and exit of the bed or at intervals along the bed length as the fluid flows. Numerous correlations can be used to obtain the pressure drop under either laminar or turbulent regime. However, while experimental and theoretical approaches obtain good approximations of pressure drop, they do not allow a more complete quantitative analysis. Hence an approach that combines these with CFD tools is highly advantageous.

2.5 Residence Time Distribution

In Chemical Engineering, the Residence Time Distribution (RTD) is one of the essential tools to consider when designing a process unit (e.g. a reactor). This methodology was developed by Danckwerts and it is used to characterize the hydrodynamics of a system and obtain basic information about the flow, in order to detect possible design flaws, such as a stagnant region, i.e. a dead zone of fluid, or a bypass behavior of a vessel (Danckwerts, 1953). The RTD is a probability function that describes the time a fluid element spends inside the system. Since CFD is capable of simulating velocity distributions and concentration fields, it is an advantageous alternative to replicate an experimental RTD study. The most expeditious way to perform an experimental RTD study is the tracer technique, which consists of injecting an inert chemical, molecule, or atom, called a tracer, into the reactor at t=0 s, and then, measuring the time evolution of the tracer concentration in the outlet, C_{out}. The injection of the tracer to the system can be made through one of four ways: a pulse input, a step input, a cyclic input, or a random input.

Providing a tracer step input is made, at the initial instant (t=0 s), the inlet flow is replaced by one with the same volumetric flow rate, but with a different tracer concentration, until steady state is reached. From the data of the transient tracer concentration at the outlet, the Danckwerts' F curve can be directly obtained by:

$$F(t) = \frac{C_{out}(t)}{C_{in}} \tag{2.10}$$

where C_{out} is the average tracer concentration at the outlet, and C_{in} is the average tracer concentration at the inlet (which is constant once the step input is started). The F curve is then the normalized concentration at the outlet obtained after a step input, which is nothing less than an average concentration evolution at the outlet.

With the $F(t)$, i.e. the response to the step input, the RTD function $E(t)$ can be obtained by:

$$F(t) = \int_0^t E(t)\, dt \quad \Leftrightarrow \quad E(t) = \frac{dF(t)}{dt} \tag{2.11}$$

which quantifies the residence time between 0 and t that the different fluid elements spend in the reactor.

Since all tracer elements will leave the unit at some point, RTD satisfies the following relationship:

$$\int_0^\infty E(t)\,dt = 1 \tag{2.12}$$

To facilitate the comparison between different flow types, it is usual to determine the F and E curves in terms of reduced time θ ($= t/\tau$):

$$E(\theta) = \frac{dF(\theta)}{d\theta} = \tau E(t) \tag{2.13}$$

where τ is the space time, determined by the ratio between the amount of fluid contained in the control volume and the volumetric flow rate passing through it.

Another important variable that could be determined from the *E* curve is the mean residence time, $\overline{t_r}$, defined as:

$$\overline{t_r} = \int_0^\infty tE(t)\,dt \tag{2.14}$$

Calculation of the $\overline{t_r}$ allows a diagnosis of the reactor flow performance by comparing its computed value to the value of τ. If $\overline{t_r} < \tau$, then there is a dead zone of fluid and/or if $\overline{t_r} > \tau$ then there is a short-circuit in the flow (a bypass).

In case there is a stagnant region, the dead volume fraction is determined by:

$$\frac{V_{stag}}{V} = 1 - \frac{\overline{t_r}}{\tau} \tag{2.15}$$

Analogously, the bypass flow rate fraction is determined by:

$$\frac{Q_b}{Q} = 1 - \frac{\tau}{\overline{t_r}} \tag{2.16}$$

where V_{stag} is the dead zone volume and Q_b is the bypass flow rate.

3 Materials and Methods

One of the main goals of this dissertation was to illustrate and characterize the effect of different operating variables (fluid velocity) and geometric parameters on the hydrodynamics of a system. For that, in the first phase, isolated CFD simulations were performed regarding the flow of a fluid with the injection of a "hot" tracer, i.e. with a higher temperature, at the entrance of the system. These simulations covered 2D and 3D geometries that present a solid structure with ordered voids defining a certain porosity. A more detailed overview of these geometries will be described in this chapter. CFD methods consist of four general steps for solving the given case: Pre-Processing, Setting Up the Simulation Case, Running the Simulation and Post-Processing. A brief insight into the CFD *modus operandi* used will be outlined in this chapter. Lastly, fully automatic optimization tests on the geometry of a 2D domain were performed. These tests were based on reaching minimum values of an illustrative and empirical objective function that translates the effect of dispersion, pressure drop and available surface area.

3.1 Pre-Processing

3.1.1 Geometry model and generation

The first step of the application of a CFD methodology to any kind of system is the creation of the mathematical domain, i.e., the system geometry. For that purpose, an adequate process for geometry modelling and generation is essential. In the present work, the geometry generation was performed with the help of Blender® software (version 2.83.0). Blender® is a free, open-source 3D computer graphics software that allows us to create files in .stl (STereoLitography) format, which are compatible with several utilities including OpenFOAM® and 3D printers. The code for the modelling and automatic generation of the geometries was made through Python™ scripting (comes bundled with Blender®).

Both 2D and 3D geometries were created with Blender® software for CFD simulations and optimization tests. This task demanded an added learning process of Blender and Python™ scripting. After being familiarized with the main concepts, a long and diligent process of implementation and improvement of the desired 2D geometries was trailed. The finished scripts allow the generation of domains filled with obstacles based on a unitary element with a chosen shape (in the present work were rectangles or ellipses) that is replicated a specified number of times and divided into two groups (represented in red in Figure 3.1). The dimensions are dependent between groups (`dimtx` in the script, which is L_x, and `dimty` in the script, which is L_y) and inclination angles (reference is the x axis) can also be set to each group (alpha1 and alpha2). For this script version, this means that it is possible to vary up to four of the geometric

characteristics of the obstacles. A demonstrative image of one of the modelled geometries showing Blender and the Python™ script can be seen in Figure 3.1.

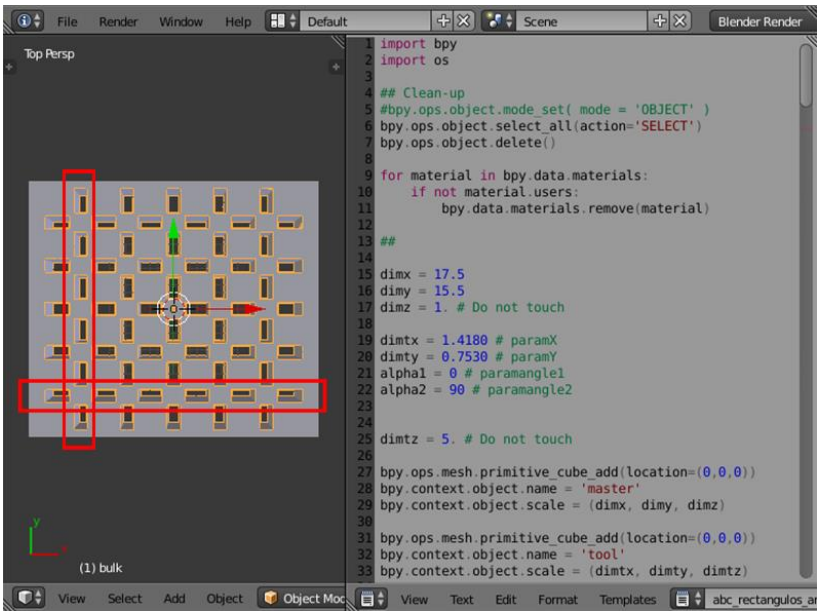

Figure 3.1-Image of Blender® console for modelling the geometry with rectangles with fixed inclination angles. The Python™ script on the right shows the domain (dimx and dimy) and geometric parameters that are being set (dimtx, dimty, alpha1 and alpha2). In this version, the inclination angles are 0°/90°. The red boxes are identifying the two sets of obstacles created.

As for the 3D geometries addressed, the Python™ script to generate the 3D structure in Blender® already existed in-house and was used after slight adaptations/modifications. These geometries consist in a bed filled with a foam structure (length of 5 cm) composed by the aggregation of unitary cubic cells. The characteristic length of a cell is 0.295 cm and the corresponding edges, normally called struts, have a diameter of 0.1 cm which imply a free distance between them of 0.095 cm (dimension used for the calculation of Re). The overall structure then suffers a double inclination of 45° that was previously found to improve the hydrodynamics of the system. It was also included a 0.2 cm buffer at both ends of the foam. The process to achieve the final structure can be seen in Figure 3.2.

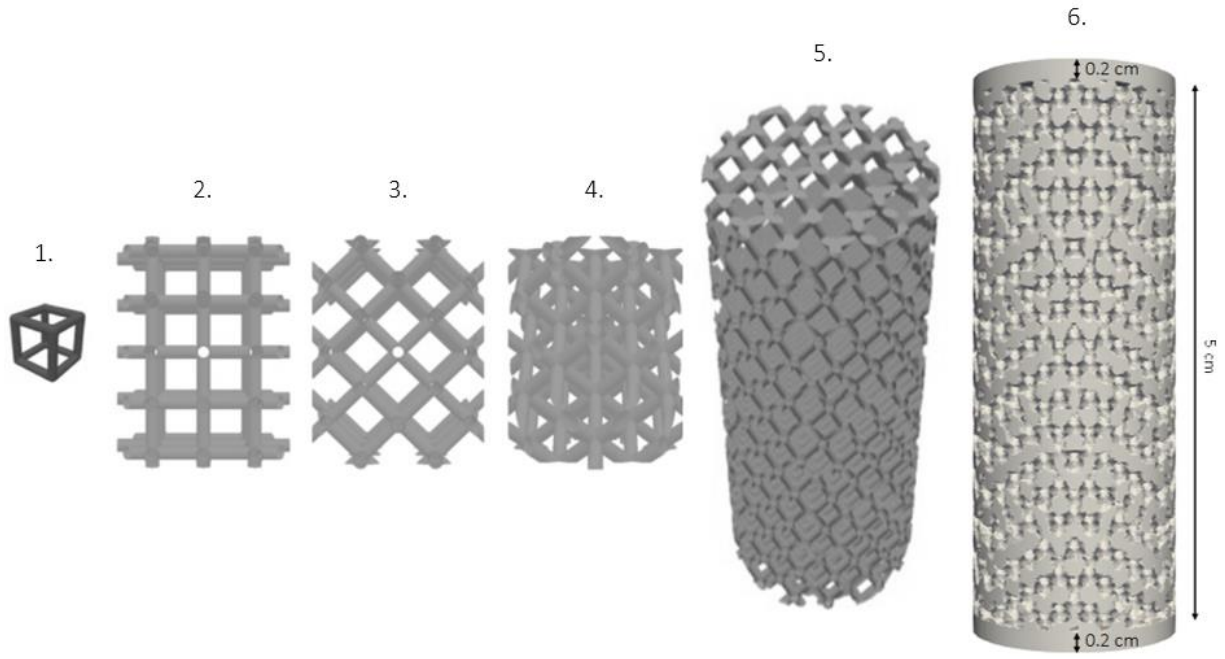

Figure 3.2-Representation of the necessary steps until reaching the 3D geometry: 1. Defining a unit cell; 2.Replication of the unit cell to create a structure; 3.Induction of an inclination of 45° in the structure; 4. Induction of a second inclination of 45°; 5. Building the foam in .stl file; and 6. Creating the simulation domain ("negative" of the foam) that defines the system volume.

3.1.2 Mesh Generation

As aforementioned, the second step of a CFD pre-processing methodology consists of dividing the mathematical domain in small elements where the model equations will be solved. This is called mesh generation and consists of replacing the continuity of the real space by several isolated points in space, the grid or mesh. In the current approach, after the .stl file is imported into the OpenFOAM® case folder and its name specified in *meshDict* file, the mesh can be generated by one of the several utilities available for the purpose. The mesh generation was made possible by the aid of CF-MESH+® version 1.1.2 for the 2D simulations, and SnappyHexMesh for the 3D simulations. CF-MESH+® is a CFD meshing product provided by Creative Fields. For the 2D simulations conducted, the CF-MESH+® tool used was `cartesian2DMesh`. SnappyHexMesh is a mesh generator supplied by OpenFOAM®. The `snappyHexMesh` utility used generates 3D meshes of hexahedral and split-hexahedral cells automatically from triangulated surface geometries.

3.2 Setting Up the Simulation Case

3.2.1 Mathematical model

As previously mentioned, in this dissertation was studied and characterized the hydrodynamics of a single-phase flow of an incompressible Newtonian fluid. For that purpose, it was used the model described in section **2.3 Governing equations (Model)** in the CFD simulations. OpenFOAM® has several base

codes implemented, having resorted to `pimpleFoam` (PISO-SIMPLE), which is prepared for incompressible systems in both laminar and turbulent regimes. This code was adapted to incorporate a few functionalities, most meaningfully the mass (2.4) and energy (2.5) equations as well as two new boundary conditions: a central core at the inlet to allow the definition of different concentration and temperature values (to replicate the injection of a hot tracer in the center of the inlet). If desired, a reaction term in the fluid (homogeneous reaction) could easily be integrated, along with its stoichiometry and reaction kinetics. The final code is compiled, and to use it, one needs to load the respective executable file created in the compilation.

3.2.2 Simulation case

After the mesh is created and the model defined, the next step in CFD simulation is the definition of the initial and boundary conditions of the different fields/variables. The files where these conditions are set are in the "0" directory of the case, as the case starts at t=0 s.

Firstly, for all the different 2D geometries, the domain, and the initial and boundary conditions used for each variable of interest are illustrated in Figure 3.3.

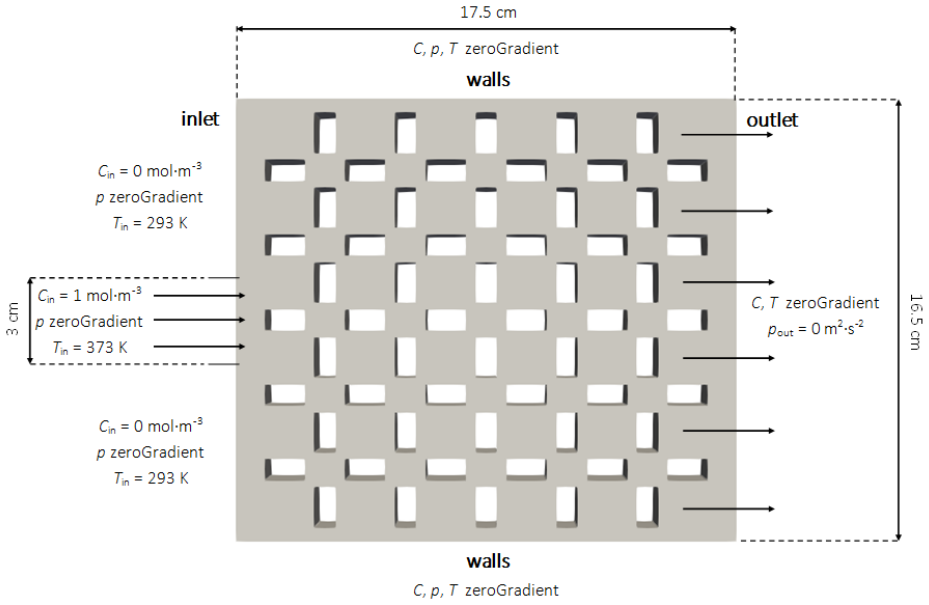

Figure 3.3-Domain for the 2D simulations (version of rectangle obstacles with 0°/90° as inclination angles) with the identification of initial and boundary conditions.

As it can be seen in Figure 3.3, the input of a tracer with 1 mol·m^{-3} and at a temperature of 373 K was simulated in the central zone of the inlet (with a width of 3 cm).

As for the 3D foam structure, the domain and the initial and boundary conditions used for each variable in the simulations are compiled in Figure 3.4.

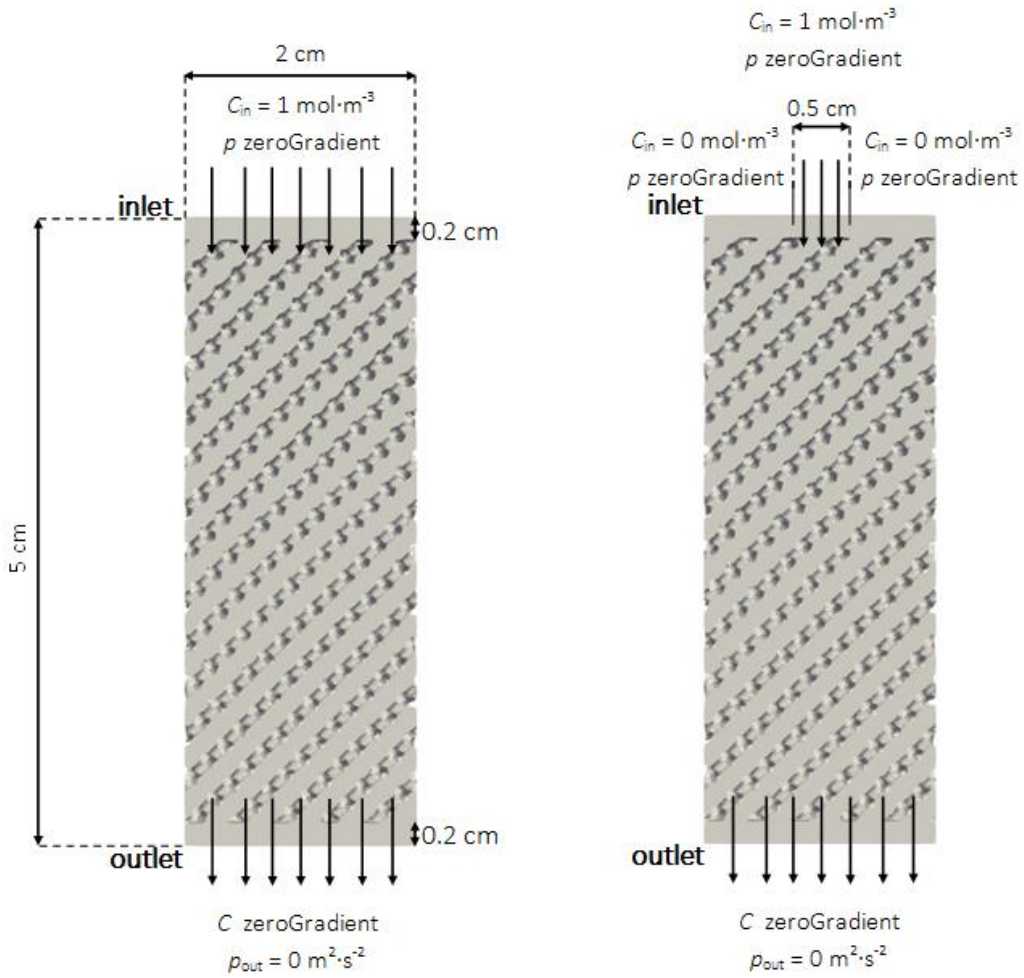

Figure 3.4-Longitudinal section view for the 3D geometries with the domain, initial and boundary conditions for the two types of simulations carried out: 1) axial tracer simulations (left) - the tracer is fed in whole cross-section; 2) radial tracer simulations (right) – the tracer feed occurs only in a central core of the inlet stream.

The physical properties of the fluids are a necessary input to solve the model equations. These properties were equivalent for both 2D and 3D simulations and were set as follows: in the "constant" directory, density, ρ, molecular diffusion coefficient, D_m, thermal diffusivity, D_T, and kinematic viscosity, ν, of the Newtonian fluid that is being modeled (typical values for water at 20°C) were defined as seen in Table 3.1.

Table 3.1-Properties of water at 20°C set on the "constant" files.

ρ / kg·m^{-3}	D_m / m^2·s^{-1}	D_T / m^2·s^{-1}	ν / m^2·s^{-1}
1000	1.0x10^{-9}	1.5x10^{-7}	1.0x10^{-6}

In the "system" directory, the numerical schemes, the convergence criteria, and the solution tolerances are assigned.

The numerical schemes related to the convection term of the governing equations, i.e. the divergence schemes, were thoroughly assigned. For the momentum equation, a `Gauss linearUpwind` scheme was chosen because it is a 2nd order scheme for vector fields, known for its stability and absence

of oscillations. As for the transport of the scalar variables (concentration and temperature), a `Gauss vanLeer` scheme was chosen since it is a specialized scheme for scalar fields. For the mass transport specifically, it was used `Gauss vanLeer01` because concentration values were bounded between 0 and 1.

As previously mentioned, the systems addressed require the simulations being performed in a transient state. As such, the time step value is variable and updated depending on a maximum Courant number between 0.1 and 0.3, following Equation (2.1).

As for the solution tolerances, they were all assigned to 10^{-7}.

Once every information and data are set in the three directories "0", "constant" and "system", it is time to run the simulation.

3.3 Running the Simulation

To begin the simulation, the name of the solver must be typed in the terminal prompt. Time directories will be created with the names of each being based on their corresponding values (or time step). The write interval to save these directories is defined in the *controlDict* file.

3.4 Post-Processing

OpenFOAM® has an embedded post-processor called ParaView®. It was used version 5.8.1. of ParaView® to visualize the numerical results of the simulations, and to extract the necessary data of the variable fields.

For each simulation performed (in 2D and 3D geometries), it was extracted the temporal variation of the average pressure at the inlet and outlet sections with the ParaView® software. Based on this numerical data, it was possible to estimate the pressure drop (an important feature for packed beds) for each flow condition.

As aforementioned, for the simulations performed in the 3D foam structure, a RTD approach was made to characterize the flow within the simulated process unit. Considering that ParaView® gives the temporal variation of the concentration, dimensionless concentration curves at the foam outlet were drawn from the data taken in the axial tracer injection simulations. The results of these curves are often combined with models of non-ideal behavior to estimate the hydrodynamic characteristics described above in chapter 2.4 Main hydrodynamic characteristics in fixed bed process units.

Regarding the estimation of D_{ax}, for the flow of a fluid through beds of stationary solid particles, is usual to assume that a piston-type of flow coupled with axial dispersion may describe reasonably such systems. For a step input, the concentration at the outlet of the bed ($z = L$) can be defined by (Danckwerts, 1953):

$$\frac{C_{out}(t)}{C_{in}} = \frac{1}{2}\left[1 - \operatorname{erf}\left(\frac{L - u_{int}t}{2\sqrt{D_{ax}t}}\right)\right] \tag{3.1}$$

where L denotes the length of the reactor and u_{int} is the interstitial velocity.

As for the radial dispersion, taking a radial co-ordinate, r, to measure the distance to the axis of the bed, and a co-ordinate z, to measure the distance along the average flow direction, the differential mass balance on the solute is given by (Delgado, 2005):

$$\frac{D_r}{r}\frac{\partial}{\partial r}\left(r\frac{\partial C}{\partial r}\right) = u\frac{\partial C}{\partial z} \tag{3.2}$$

A solution of Equation (3.2) that considers the tracer to be of significant diameter compared to the diameter of the bed (See Annex A) and considering that D_r and u are independent of position, the resulting outlet average concentration in the inner stream is given by (Hiby and Schummer, 1960):

$$\frac{C_{out}(t)}{C_0} = 4\sum_{n=0}^{\infty}\frac{J_1^2(\lambda_n R_i/R)}{\lambda_n^2 J_0^2(\lambda_n)}\exp\left[-\frac{LD_r}{u_{int}}\left(\frac{\lambda_n}{R}\right)^2\right] \tag{3.3}$$

where J_0 and J_1 are the Bessel function of the first kind, of orders 0 and 1, respectively, λ_n denotes the positive roots of the Bessel functions of the first kind, of order 1, R_i is the tracer injection tube radius, and R is the radius of the packed bed. The tracer concentration at the outlet central region, C_{out}, and the tracer concentration in the radial inlet injection zone, C_0, provides a prompt method for the determination of D_r, since all other parameters in the equation are previously known.

With the help of ParaView®, the values taken from slices slightly above and below the foam (in the upper and lower buffer) were exported to Microsoft Excel. These values were then integrated to obtain the average concentration at these cross-sections. Repeating this methodology for each time step, the simulation ***F*** curves can be plotted. Adjusting these curves to equation (3.1) using the least-squares method via Microsoft Excel's *solver* tool allowed to estimate D_{ax}. For the D_r specifically, a similar procedure was done but only for the final time step and applied to the core of these sections with a radius equal to the injection radius. This will give a single value of $\bar{C}/C_0$ (for each simulation) to compare with equation (3.3) and obtain the radial dispersion.

3.5 Optimization approach

Firstly, an in-house fully automatic iterative optimization methodology was improved and adapted to the two-dimensional systems addressed in the simulations and described in sections 3.1, 3.2, 3.3 and 3.4. This methodology consists of coupling the previous four steps (geometry generation, meshing, CFD simulation and post-processing) with an optimizer and, based on a pre-established objective function, creating an iterative process to find optimal solutions. The optimizer used was Nomad® version 3.8.0.

So, the optimization procedure incorporates the whole process that has been described and executed up until now in a sequential manner. The procedure starts with the input of an initial estimate for the values of the geometric parameters to optimize – this is the only action required to the user since the process is fully automatic. Then, within a loop, after the CFD simulation ended and the necessary data is post-processed, the optimizer evaluates whether its geometric parameters comply with a designated goal (minimize the objective function) or not. If not, then it generates new values for these geometric parameters and the process is repeated until the goal is achieved. A block diagram of the optimization procedure can be seen in Figure 3.5.

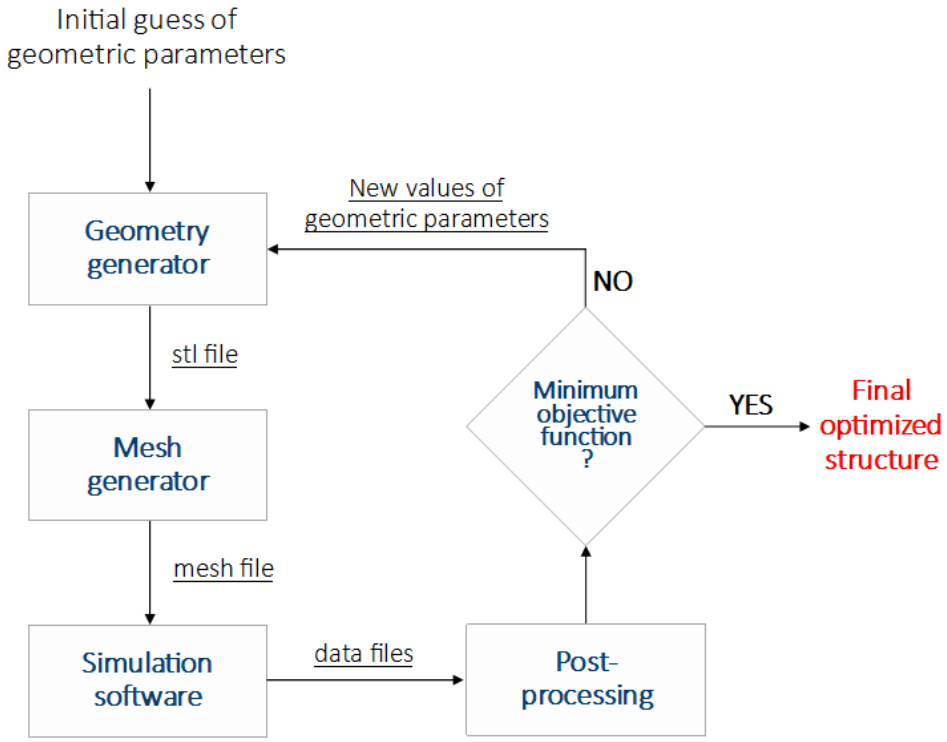

Figure 3.5-Block diagram of the optimization procedure.

The specific data obtained in the post-processing is oriented to calculate an objective function, F_{obj}, that must be previously chosen/defined in the code and must address the specificities/limitations of the system. In the present work, the F_{obj} was defined empirically for illustrative purposes, and involves simple features to roughly quantify dispersion, pressure drop, and solid surface area per unit of total volume of the system:

$$F_{obj} = \underbrace{w_C \frac{\sum|C_{out} - \overline{C_{out}}|}{\overline{C_{out}}}}_{\text{mass dispersion}} + \underbrace{w_T \frac{\sum|T_{out} - \overline{T_{out}}|}{\overline{T_{out}}}}_{\text{heat dispersion}} + \underbrace{w_p(-\Delta p)}_{\text{pressure drop}} + \underbrace{w_A \frac{V_{total}}{A_s}}_{\text{surface area}} \quad (3.4)$$

where the parameters w_C, w_T, w_p and w_A are the weights of each term in the objective function. The goal is to minimize the objective function, i.e. to minimize the terms defined to assess dispersion (mass and heat), minimize the pressure drop, and maximize the surface area (A_s), which is why the latter is in the denominator. The term regarding the surface area is specifically useful if one wants to implement this optimization procedure to a catalytic reactor, since a greater surface area of the catalyst favors the reaction rate.

4 Results and Discussion

4.1 CFD Simulations with 2D geometries

4.1.1. General overview

As previously mentioned, the structures addressed in the 2D simulations are composed by obstacles with a pre-defined topology, and have a total length of 17.5 cm (in x direction) and a width of 16.5 cm (in the y direction). For reference purposes, it was chosen a structure filled by rectangular obstacles with a length (L_x) of 1.418 cm and a width (L_y) of 0.753 cm (in order to make up for a porosity of 0.75) and inclination angles of 0º and 90º. Simulations replicating the injection of a hot tracer and considering laminar flow model were performed on this geometry with different inlet velocities. Once the simulations are over, CFD post-processing returns the fields of the variables in the model (concentration, temperature, velocity, and pressure). Starting the analysis of results by the case with an inlet velocity of 0.17×10^{-2} m·s^{-1}, the fields can be seen in Figure 4.1 for the final simulation time of $2.5 \cdot \tau$, with τ being 80 s. This velocity case corresponds to a Reynolds number of 50, whose characteristic dimension is the width of the central inlet (3 cm).

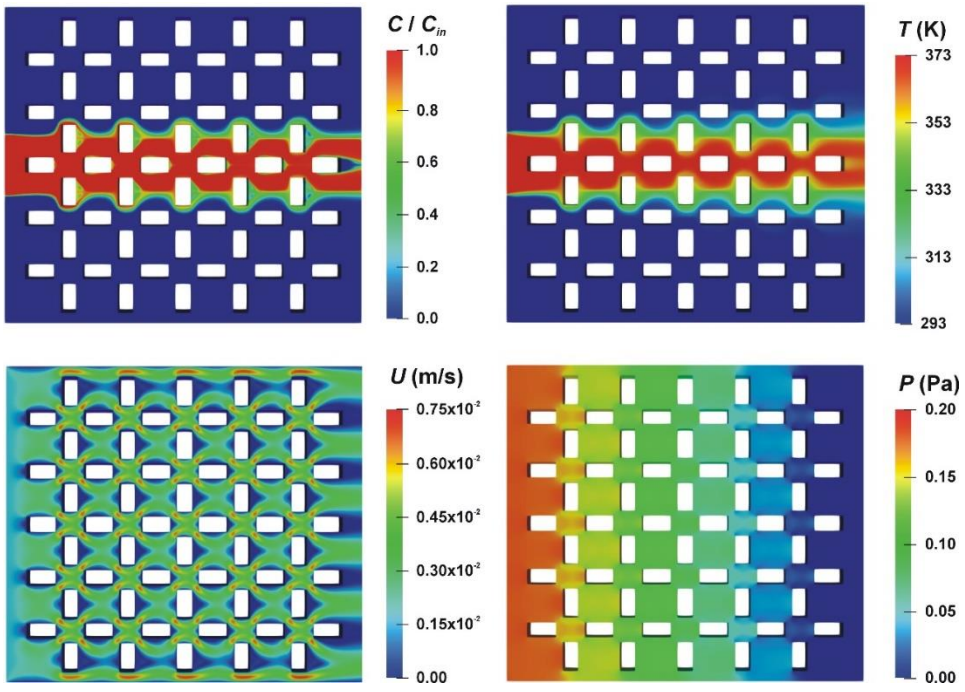

Figure 4.1-Dimensionless concentration (upper left), temperature (upper right), velocity magnitude (lower left) and pressure (lower right) fields obtained at the end of the simulation ($2.5 \cdot \tau$, with τ = 80 s) performed for the geometry with rectangular obstacles and a $U_{in} = 0.17 \times 10^{-2}$ m·s^{-1} (Re = 50). The geometry considered is the rectangular 0°/90° obstacles with L_x = 1.418 cm and L_y = 0.753 cm.

By looking at the concentration and temperature fields in Figure 4.1, one can infer that the flow promotes a poor level of mixing, since the tracer does not spread for areas outside the one defined by the central injection region (small communication between neighboring fluid elements). In addition, when

comparing these two fields, it is possible to notice that the thermal dispersion seems to be slightly higher, which is due to the fact that the thermal diffusivity is larger than the mass diffusivity (by a factor of 1.5×10^2). Despite this, the effect is not very significant, and the visual analysis of the mixing level can be based on both C and/or T fields. Regarding the velocity field, it can be identified zones where the velocity is null suggesting the presence of stagnant regions, which are more pronounced in the obstacles closer to the walls. One can also observe that the magnitude values reach a maximum of almost 5 times the average inlet velocity. As for the pressure field, the pressure drop seems to be relatively low (has a maximum value of 0.20 Pa) and evolving linearly with the distance travelled by the flow.

The CFD post-processing allows to follow the temporal behavior of the variable fields. In Figure 4.2, it can be seen the representation of the dimensionless concentration fields for various time instants, which provide a good perspective on the evolution of this variable.

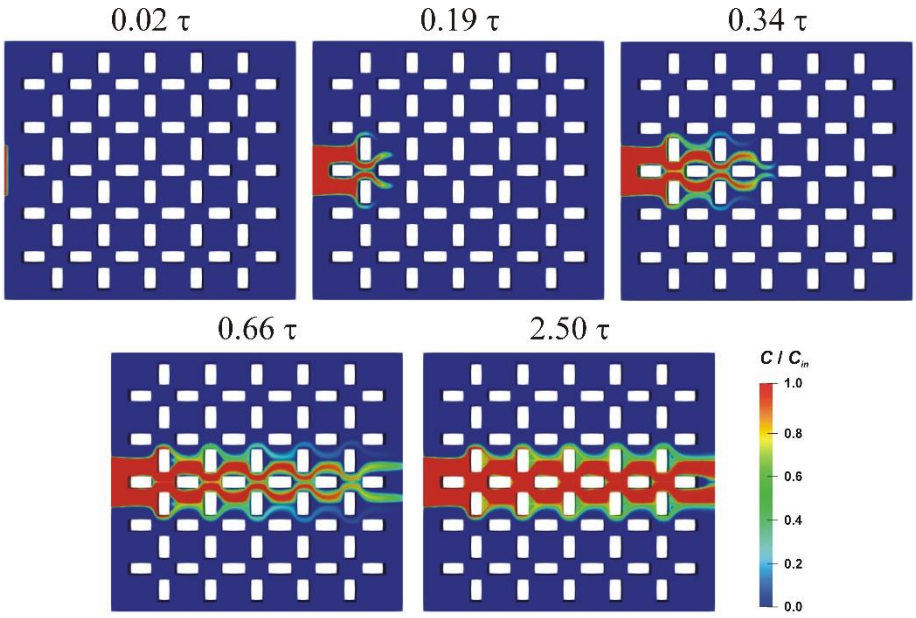

Figure 4.2-Temporal evolution of the concentration field for the geometry with rectangular obstacles and with U_{in} = 0.17x10^{-2} m·s^{-1} (Re = 50). The space time (τ) for this velocity is 80 s. The geometry considered is the rectangular 0°/90° obstacles with L_x = 1.418 cm and L_y = 0.753 cm.

Figure 4.2 shows that the tracer would flow through half of the structure in 0.34·τ s, and would reach the outlet at around 0.66·τ s. This proves that a simulation time of 2.5·τ s is more than enough to assume that a steady state is achieved in these systems.

4.1.2 Inlet velocity effect

As aforementioned, simulations were performed for a set of different inlet velocities, in order to assess the effect of this operating variable in the hydrodynamics of the flow through the 2D geometries under the scope. The corresponding Reynolds number ranges from 25 to 300. In Table 4.1 are presented the different inlet velocities used in the 2D simulations.

Table 4.1-Inlet velocities, corresponding Reynolds number and space times for each of the 2D structures.

	1	2	3	4
U_{in} / m·s^{-1}	0.083x10^{-2}	0.17x10^{-2}	0.50x10^{-2}	1.00x10^{-2}
Re	25	50	150	300
τ / s	160	80	27	13

Focusing on the same 2D geometry addressed in the previous sub-section, the numerical results of the dimensionless concentration fields obtained for each Reynolds number are plotted in Figure 4.3.

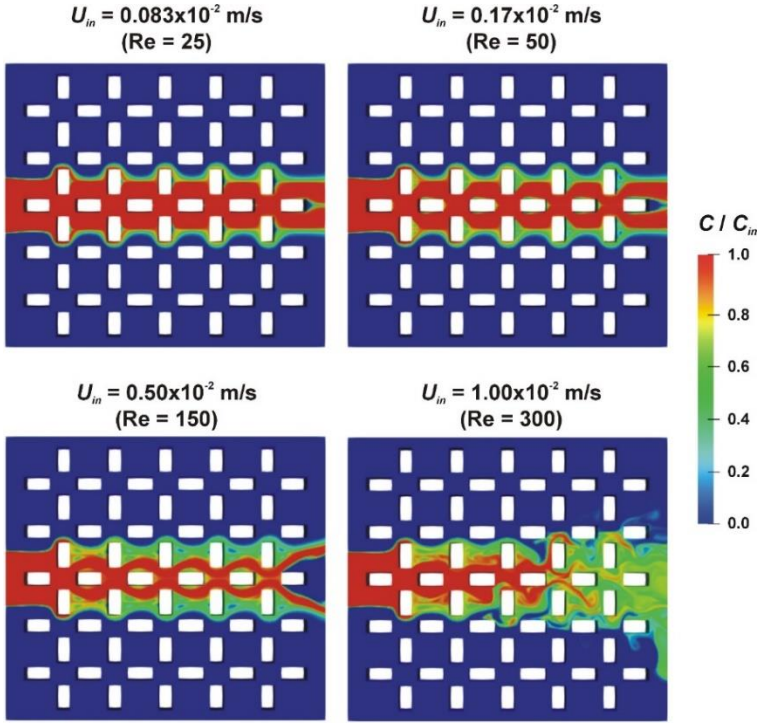

Figure 4.3-Dimensionless concentration fields at the end of the simulation for each Reynolds number. The geometry considered is the rectangular 0°/90° obstacles with L_x = 1.418 cm and L_y = 0.753 cm.

By observing Figure 4.3, for the three lower simulated Reynolds numbers (25, 50 and 150), it can be checked that the concentration fields clearly suggests preferential paths, since all of the tracer exits the domain through the middle region of the outlet. The concentration data at the outlet was extracted from these fields, and the corresponding C/C_{avg} profiles drawn and plotted in Figure 4.4 (with C_{avg} been the average concentration at the outlet).

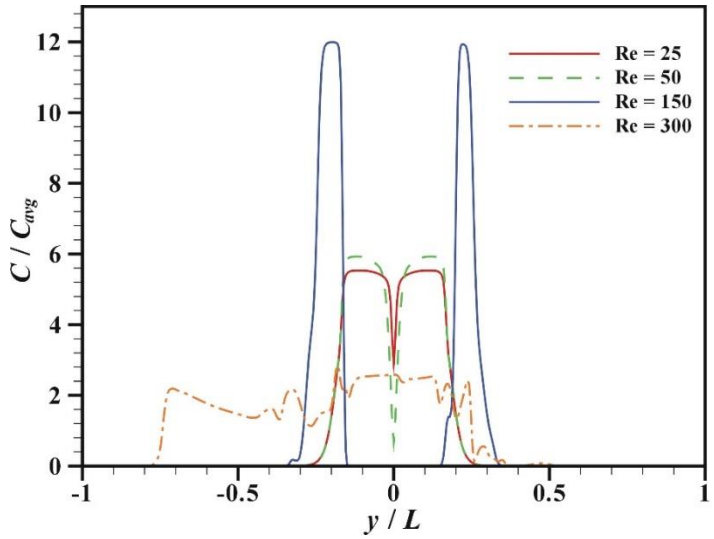

Figure 4.4- Outlet concentration profiles at the end of the simulation for each Reynolds number. The geometry considered is the rectangular 0°/90° obstacles with L_x = 1.418 cm and L_y = 0.753 cm.

As previously visualized in Figure 4.3, the concentration distribution at the outlet is very similar for the two lower Reynolds numbers (25 and 50). The profile for Re = 150 shows two y/L regions where all the tracer concentrates, which reinforces and intensifies the identification of clear preferential paths. As for Re = 300, Figure 4.4 indicates that most of the tracer leaves the structure by the bottom half of it (y/L < 0), but also gives the perception that the flow has instabilities and a clear steady state was not achieved. Due to this last point, the concentration fields for times close to the end of the simulation are represented in Figure 4.5, in order to evaluate if there is a stabilization of the flow.

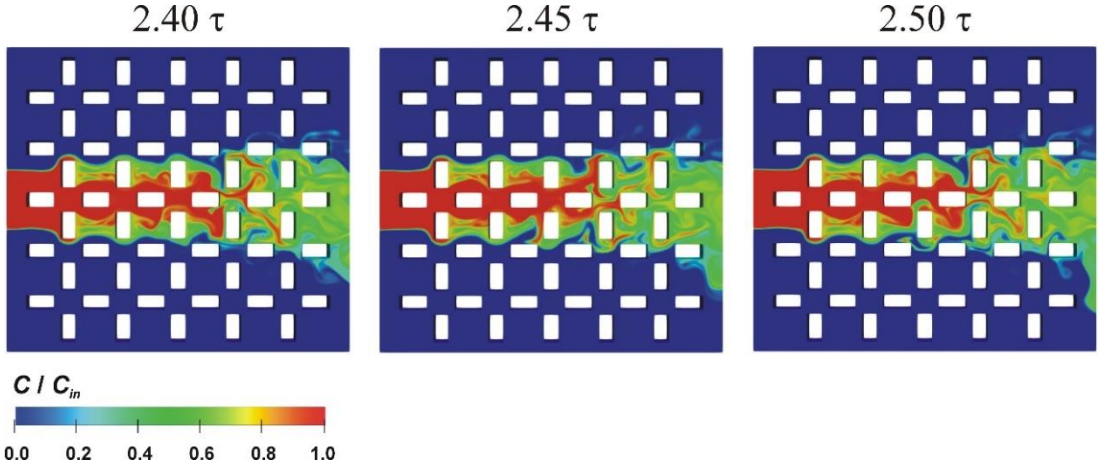

Figure 4.5-Concentration fields for times near the end of the simulation for Re = 300. The geometry considered is the rectangular 0°/90° obstacles with L_x = 1.418 cm and L_y = 0.753 cm.

For the physical time simulated (2.5·τ, with τ being 13 s), it seems that a full stabilization of the flow does not happen for an inlet velocity of 0.01 m/s. A possible explanation is that the flow instabilities generated in this system can be caused by a sort of wall effect and become a periodic phenomenon. It would be very interesting to further investigate this phenomenon, but it would need simulations with larger

domains and a more detailed temporal analysis. However, this task is outside of the scope of the present thesis.

4.1.3 Geometry effect

As discussed in chapter **2.4.1 Axial and Radial Dispersion,** dispersive effects and pressure drop are dependent on the geometry of the structure. So, besides the structure addressed in sections 4.1.1. and 4.2.1., other three 2D geometries were created (two with ellipsoidal obstacles and other with rectangular obstacles) so that it could be inferred if a different level of mixing and pressure drop was obtainable. In order to produce a more meaningful comparative evaluation of the four geometries, the geometrical parameters where set so that the surface area of the ellipses were equal to the surface area of the rectangles. The geometric parameters set are shown in Table 4.2.

Table 4.2-Geometrical parameters of the obstacles in the four 2D structures (L_x ≡ length; L_y ≡ width; r_1 ≡ semimajor axis; r_2 ≡ semiminor axis; α_1 ≡ rotation angle 1; α_2 ≡ rotation angle 2).

		
2 parameters	L_x = 1.418 cm L_y = 0.753 cm	r_1 = 1.6 cm r_2 = 0.85 cm
4 parameters	L_x = 1.418 cm L_x = 0.753 cm α_1 = 45° α_2 = 135°	r_1 = 1.6 cm r_2 = 0.85 cm α_1 = 45° α_2 = 135°

The steady-state dimensionless concentration field obtained for each of the four 2D structures with an average inlet velocity of 0.17×10^{-2} m·s^{-1} (Re = 50) can be seen below in Figure 4.6.

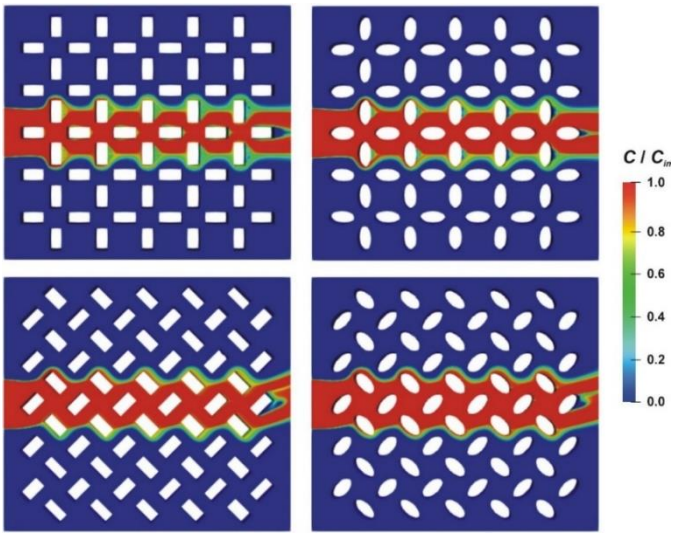

Figure 4.6-Steady-state dimensionless concentration field obtained for each of the four geometries with U_{in} = 0.17×10^{-2} m·s^{-1} (Re = 50) at the end of the simulation (2.5·τ, with τ = 80 s for the rectangular geometries (left images) and τ = 72 s for the ellipsoidal geometries (right images)).

For the Reynolds number of 50, the numerical results in Figure 4.6 suggests that the variation made in obstacles geometry is almost not affecting the level of mixture. As it was inferred before, tracer elements are also taken preferential paths in the new three geometries. It was found previously that the mixing benefited from a higher Reynolds number of 300 (due to flow instabilities). So, the dimensionless concentration fields obtained for each of the four geometries with U_{in} = 1.00x10^{-2} m·s^{-1} are represented below in Figure 4.7. The intention was to somehow amplify the level of tracer spreading in order to facilitate the assessment of the geometry effect on the dispersion/mixing level.

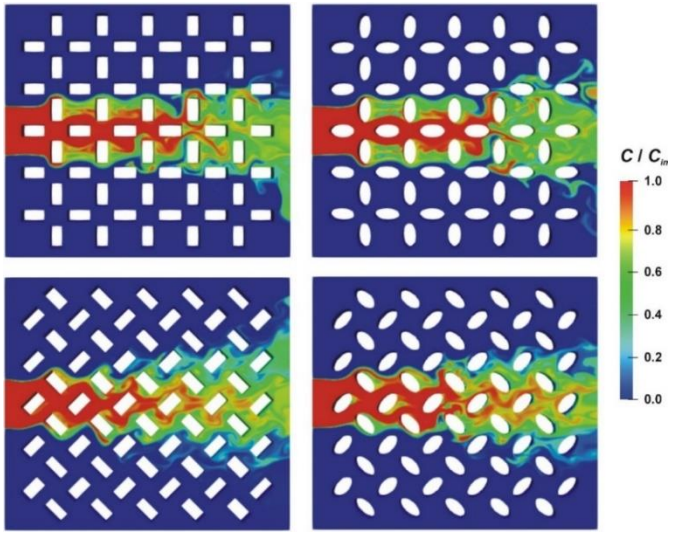

Figure 4.7-Dimensionless concentration field obtained at the end of the simulation (2.5·τ, with τ = 13 s for the rectangular geometries (left images) and τ = 12 s for the ellipsoidal geometries (right images)) for each of the four geometries with U_{in} = 1.00x10^{-2} m·s^{-1} (Re = 300).

In Figure 4.7, it can be observed that in fact, all geometries demonstrate a higher level of mixing for this inlet velocity condition. Additionally, the concentration fields also suggest that there is a potential for best performances in terms of mixing with the rectangular and inclined obstacles (the tracer elements disperse to a larger zone outside the central region of injection).

The outlet dimensionless concentration profiles versus y/L were also plotted. These are shown in Figure 4.8 for all simulations, i.e., for the four geometries and each geometry in the four Reynolds numbers simulated.

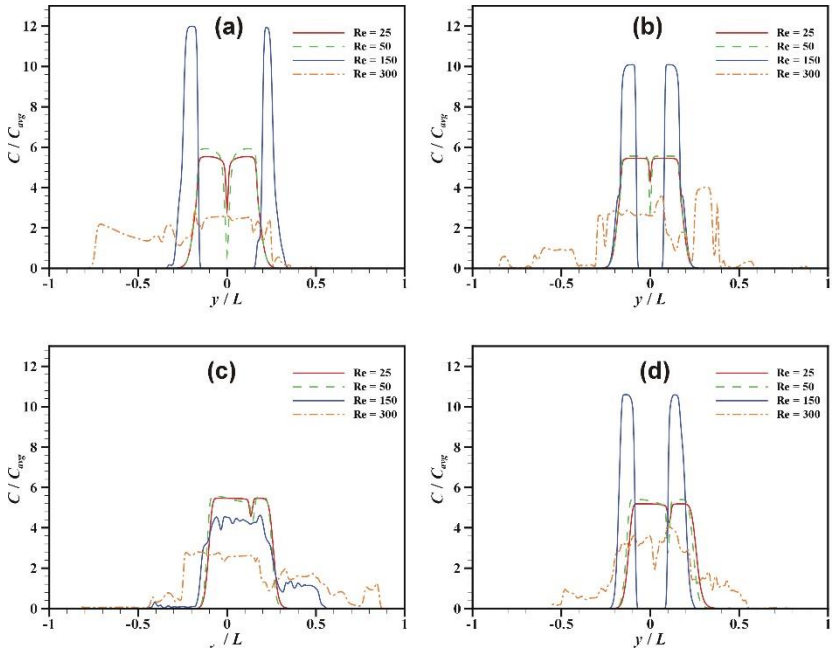

Figure 4.8- Dimensionless concentration profiles at the outlet obtained for all the geometries and inlet velocity conditions addressed: (a) rectangles 0°/90°, (b) ellipses 0°/90°, (c) rectangles 45°/135°, (d) ellipses 45°/135°.

The qualitative evaluation made with Figure 4.7 is confirmed by the observation of Figure 4.8, i.e., overall, the structure with rectangular obstacles at 45°/135° is the one that provides a higher concentration dispersion. In terms of mixing, the inclined rectangular topology is preferable to the corresponding ones with ellipses obstacles.

As explained in previous sections, the pressure drop is another important feature to take into consideration when assessing the effect of the structure geometry. As such, it is intended to assess for which geometry the loss of energy from the flow of the fluid is the lowest. For that purpose, the pressure drop per unit length for the four illustrative 2D geometries are plotted in Figure 4.9 as a function of Re.

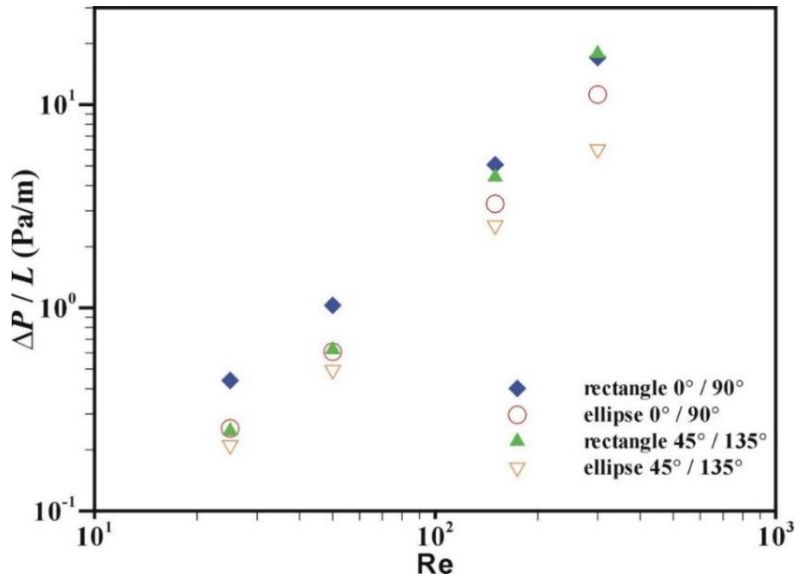

Figure 4.9-Pressure drop per unit length for the four illustrative geometries as a function of Re.

As expected, pressure drop per unit length increases with the increase of the values of Reynolds number. Furthermore, the most important information to take from Figure 4.9 is that there is a tendency for pressure drop to be lower for more inclined obstacles (45°/135°), both in rectangular and ellipsoidal topologies. The only exception seems to be for the two rectangular options at the highest Reynolds number (perhaps caused by the oscillations and instabilities previously referred for this velocity condition). Nonetheless, it is clear that the most favorable topology in terms of pressure drop are the ellipses, i.e., with the lowest ΔP for all the inspected values of Re number. This conclusion was somehow predictable due to the absence of sharp corners (present in rectangles), that offer higher flow resistance and frictional energy losses.

From the analysis of the geometry effect, it was noticed that a rectangular topology is preferable in terms of mixture, while in terms of pressure drop, geometries with ellipse obstacles are favored. Since the mixing level observed in the rectangular geometries is significantly better, while the differences in pressure drop are not so jarring between the two types of geometries, it was decided to use the rectangular topology in the subsequent optimization tests.

4.2 CFD Simulations with 3D geometries

4.2.1. General overview

The mathematical domain addressed in the 3D simulations is a structure that features two types of regions: 1) a porous space between the foam structure and the walls with a length of 5 cm and a porosity of 0.56. The geometrical characteristics of the foam and its generation were described in section 3; 2) two buffers, at the inlet and outlet, of 0.2 cm each, that provide stability to calculations and a better definition of the tracer inlet conditions. Laminar flow simulations with different inlet velocities were performed to replicate two types of tracer experiments in the 3D geometries: 1) step input in the entire inlet cross-section to assess axial dispersion (will be called “axial tracer”); 2) step input in a central region of the inlet to assess radial dispersion (will be called “radial tracer”). Starting the 3D simulations analysis with a radial tracer injection and an inlet velocity of 0.10 $\mathrm{m \cdot s^{-1}}$, the concentration, velocity, and pressure fields obtained after a simulation time of $3.0 \cdot \tau$ can be seen in Figure 4.10, with τ being 0.28 s. The Reynolds number of the fluid ($\mathrm{Re_f}$), computed based on the free distance between struts (0.095 cm), is 95.

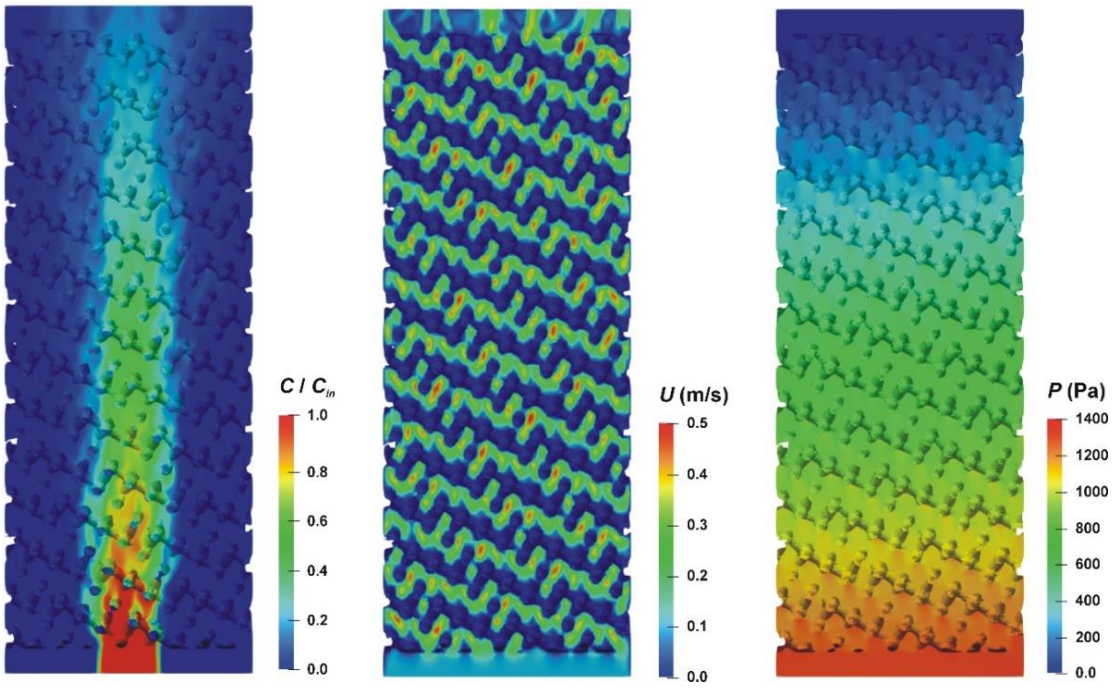

Figure 4.10- Dimensionless concentration (left), velocity magnitude (middle) and pressure (right) fields obtained with U_{in} = 0.10 m·s^{-1} (Re_f = 95) (view of a longitudinal cut of the 3D geometry). These numerical results were obtained for the simulation with central tracer injection at 3.0·τ, with τ = 0.28 s.

From the fields presented in Figure 4.10, it is possible to get an overall "picture" of the behavior of the main variables. Starting from the dimensionless concentration field (left), in qualitative terms, it can be said that some radial dispersion is occurring. As for the velocity magnitude, it increases to a maximum of 5 times the inlet velocity (0.1 m·s^{-1}) in some regions, and also some spots with low velocity (close to zero) suggest the possibility of small stagnant volumes. Regarding the pressure field (right), for an inlet velocity of 0.1 m/s, the pressure drop is in the magnitude range of about 10^3 Pa.

The temporal evolution of the tracer concentration in the two types of referred simulations is also a relevant information that is possible to visualize. So, for an inlet velocity of 0.10 m·s^{-1}, tracer concentration fields for various instants are represented in Figure 4.11.

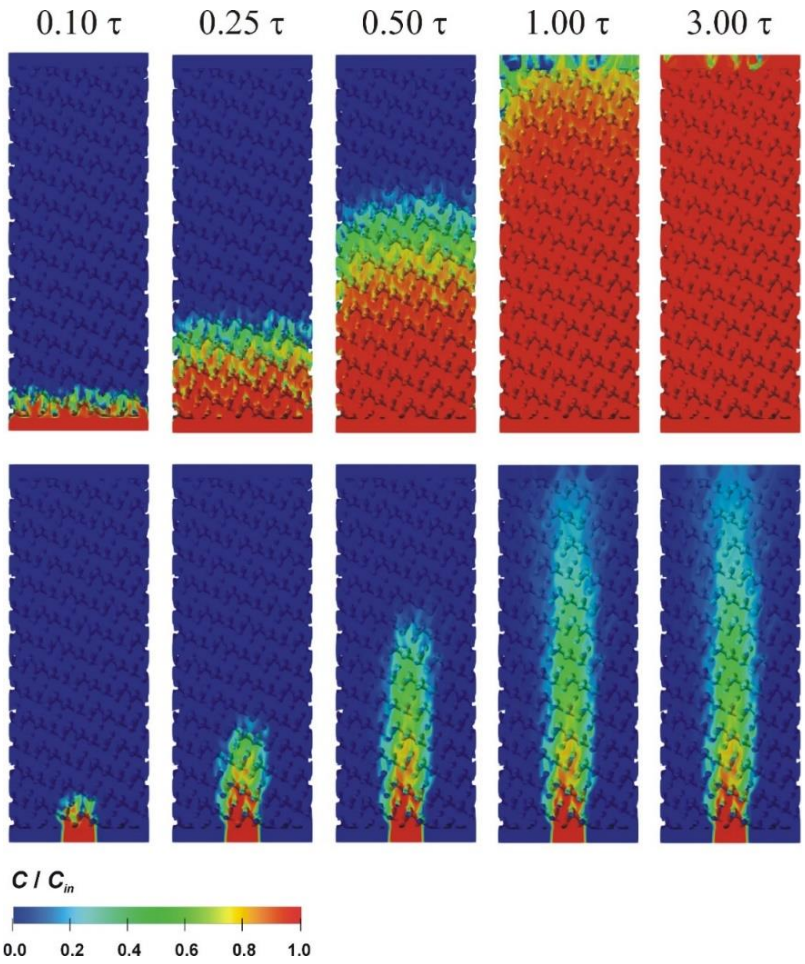

Figure 4.11-Temporal evolution of the concentration fields for the axial tracer (upper images) and radial tracer (bottom images) simulations with U_{in} = 0.10 m·s^{-1} (Re_f = 95) (view of longitudinal cuts of the 3D geometry).

It can be observed that, for both types of tracer inlets, the concentration front passed through half of the structure at 0.50·τ and, at 1.00·τ, the tracer already reached the end of the structure. This is indicative of the expected non-ideality of the system, that is, the presence of an axial dispersion instead of a purely piston-type of flow. In fact, the upper images of Figure 4.11 show some green color above the concentration front (in red), which is a sign that there is presence of axial dispersion. As for the bottom images, it can be seen that radial dispersion becomes more and more visible as the concentration front moves along the foam.

4.2.2 Inlet velocity effect

In order to assess the effect of the inlet velocity in the flow hydrodynamics, several simulations were performed for different values of Reynolds numbers (presented in Table 4.3).

Table 4.3-Inlet velocities, corresponding Reynolds number and space times for each of the simulations with 3D geometries.

	1	2	3	4	5	6
U_{in} / m·s^{-1}	0.010	0.020	0.050	0.067	0.100	0.167
$\mathbf{Re_f}$	9.50	19.0	47.5	63.4	95.0	158
τ / s	2.80	1.40	0.56	0.42	0.28	0.17

The steady-state concentration fields obtained in the radial tracer simulations can be seen in Figure 4.12.

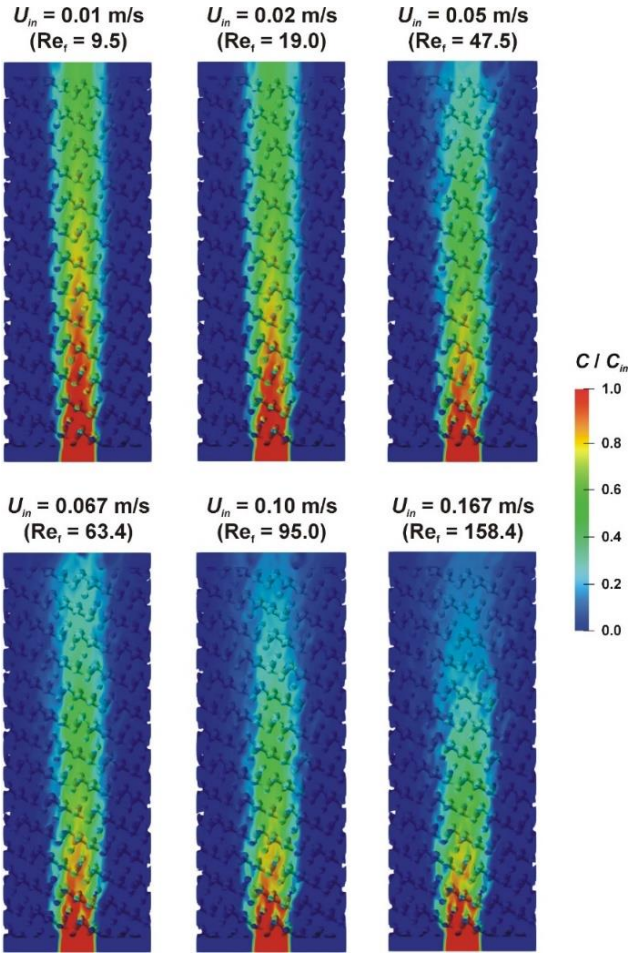

Figure 4.12-Steady-state tracer concentration fields obtained in the radial tracer simulations for different inlet velocities (view of longitudinal cuts of the 3D structure).

From the observation of Figure 4.12, velocity appears to favor radial dispersion, since for higher flow velocities, a greater distribution of tracer is visible outside the central zone of injection.

Based on the numerical data obtained in the axial tracer simulations, it is possible to build the corresponding $F(t)$ curves according to the RTD theory and the methodologies described in chapter **2.5 Residence Time Distribution**. These results were obtained for the different inlet velocity conditions and can be seen in Figure 4.13 after being converted into $F(\theta)$ version (with the exception of one condition – Re of 63.4 – to diminish the overlapping and facilitate visualization).

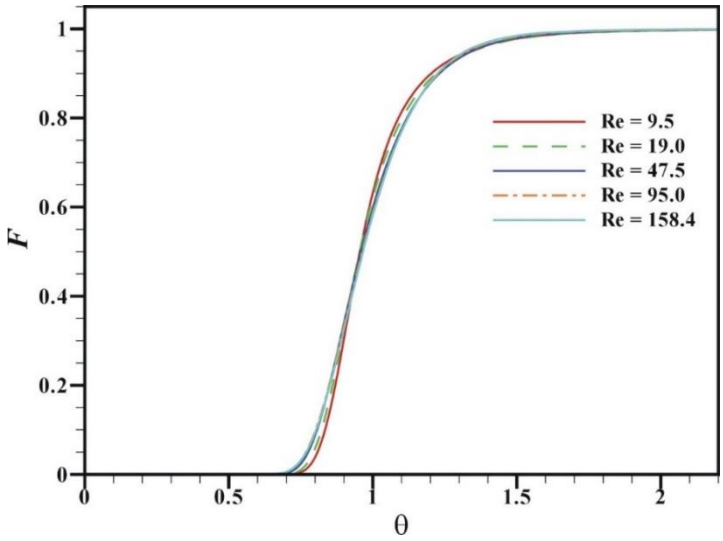

Figure 4.13- $F(\theta)$ curves based on the simulation results for different Reynolds numbers.

From the observation of the $F(\theta)$ curves in Figure 4.13, it can be claimed that velocity (ergo Reynolds number) has an influence on dispersion since the curves are not fully overlapped. For example, with Re = 158.4, tracer starts to exit the structure at θ = 0.69, while with Re = 9.5 this happens only at θ = 0.75.

4.2.3 Dispersive analysis

It was seen above that the simulated systems show clear signs of dispersion. As such, the coefficients of dispersion, D_{ax} and D_r, are computed by adjustment to the equations already presented in chapter 3.4 Post-Processing:

- t_{stag} was added to Equation (3.1) as an adjustment parameter, since it was suspected that there were stagnant volumes. The resulting equation is given by:

$$F(t) = \frac{1}{2}\left[1 - \text{erf}\left(\frac{L - u_{int}(t + t_{stag})}{2\sqrt{D_{ax}(t + t_{stag})}}\right)\right] \quad (4.1)$$

The simulation $F(t)$ curves were adjusted to these two-parameter function and an example can be seen in Appendix E.

- D_r comes from adjusting the steady-state $C_{out}/\ C_0$ value in the core (obtained by simulation) with Equation (3.3).

The plot in logarithmic scale of D_{ax}/D_m and D_r/D_m versus Reynolds number of the fluid for each simulation can be seen in Figure 4.14, as well as the percentage of stagnant volume.

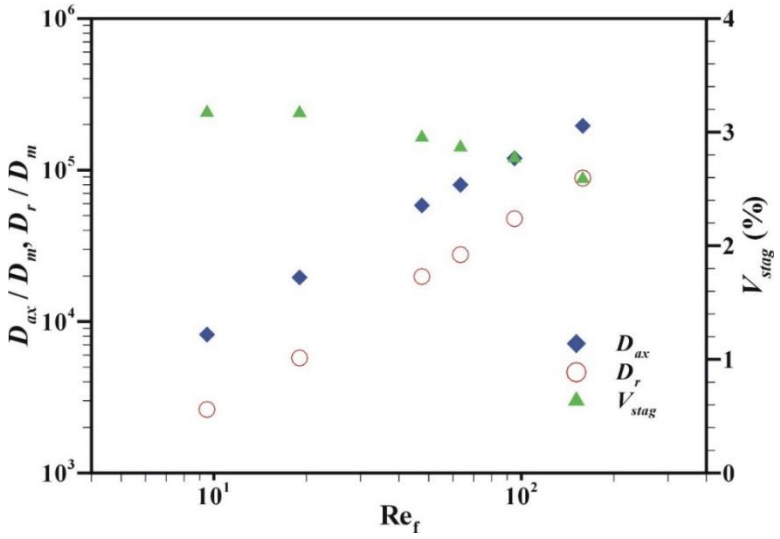

Figure 4.14-Numerical estimations of the dimensionless dispersion coefficients (axial and radial) and percentage of the stagnant volume as a function of Re_f.

Since dispersion is normally anisotropic, i.e. it assumes different values depending on the direction being taken into account, it was expected that the values obtained for the axial dispersion coefficient (D_{ax}) would be different from the radial dispersion coefficient (D_r). In this specific 3D geometry, D_{ax} is higher than D_r for all of the inlet velocity conditions simulated (i.e., $\mathrm{Re_f}$ numbers). From Figure 4.14, it can also be concluded that both the dispersion coefficients increase with the increase of the Reynolds number, which was already predictable according to the literature (Delgado, 2005). The values of estimated percentage of stagnant volume, however, are lower when compared to the ones obtained for a similar geometry subjected previously to in-house studies (Barbosa, 2019), see Annex B. As for a tendency, it can be seen that up to a certain $\mathrm{Re_f}$ value there is some stability in the percentage of stagnant volume, whereas for high Reynolds numbers, V_{stag} decreases with the increase of the flow velocity.

4.2.4 Pressure drop analysis

Based on the pressure fields obtained in the 3D simulations, the corresponding pressure drop values were computed according to chapter **2.4.2 Pressure Drop**. The numerical values obtained (per unit length) are plotted as a function of Reynolds number in Figure 4.15. Additionally, it is also represented a fitted pressure drop curve following the functionality of Equation (2.9).

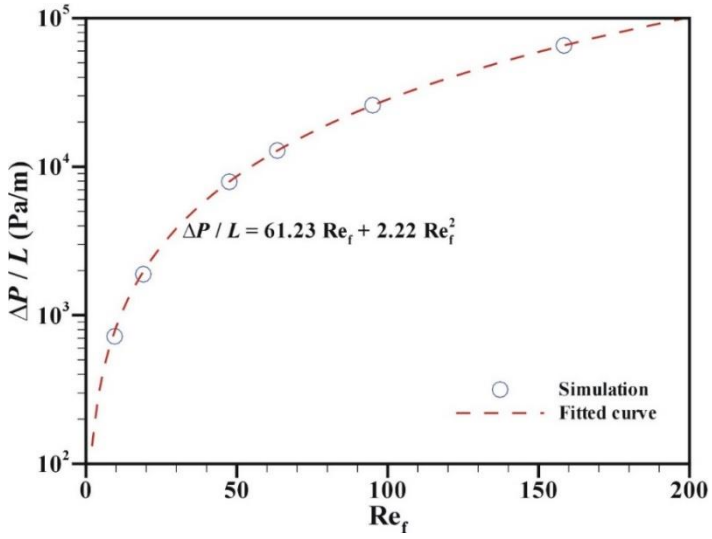

Figure 4.15-Numerical pressure drop per unit length in logarithmic scale as a function of Reynolds number (Simulation). Fitted curve of pressure drop as a function of Reynolds of the fluid that was also obtained following *Ergun* equation.

Firstly, and as expected, the pressure drop grows with the increase of the average inlet velocity. The flow is indeed laminar as the left term (corresponding to the Kozeny-Carman term) of the fitted curve expression is higher than the right term by a factor of about 28. The fitted curve based on equation 2.9 adjusts very well to the simulation results. This suggests that the corresponding expression could be used to estimate pressure drop in this foam structure for other non-simulated Reynolds numbers (within the range of 9.5 to 158).

4.3 Optimization tests

Optimization tests were performed with the 2D geometries composed by rectangular obstacles (with variation of 2 and 4 geometrical parameters). This option was based on the fact previously observed in chapter **4.1.3 Geometry effect** that the rectangular obstacles have a higher potential (in comparison with ellipses) to promote a better mixing. Ideally though, similar optimization tests should be repeated for both topologies. However, due to time issues, it was not feasible to address also the 2D geometries with ellipsoidal obstacles during this thesis, since typically each optimization may involve hundreds of CFD simulations. The same reason applies to avoiding the 3D geometries in the optimization tests, as these involve much heavier geometry generation and CFD simulations.

The optimization tests start by setting the initial guess values of the geometrical parameters. For all tests, these values were: L_x and L_y of 1 cm; α_1 of 0º; and α_2 of 90º. The admissible ranges for both L_x and L_y were 0.3 cm to 2.0 cm in all optimization tests, but α_1 and α_2 are only variable (between 0º and 180º) for the test with optimization with 4 geometrical parameters.

The velocity conditions and weights of the F_{obj} used in the optimization tests are expressed in Table 4.4. The intention is minimize the objective function (Equation 3.4) and evaluate the effect of the weights on its terms.

Table 4.4-Assigned weights for each term of the objective function for the five optimization tests performed.

N° geometric parameters	U_0 / m·s^{-1}	w_C	w_T	w_p	w_A
2	0.002	2	75	0.75	100
		2	75	50	100
	0.01	2	75	0.75	100
		2	75	15	100
4	0.002	2	75	0.75	100

Firstly, the optimization test in the first line of Table 4.4 was performed, i.e., with 2 geometric parameters, U_{in} of 0.002 m·s^{-1} and a w_P of 0.75. The L_x and L_y obtained in each iteration, and the ratio between the F_{obj} in each iteration and the corresponding F_{obj} for the initial guess (in order to easily perceive if there is improvement or not along the optimization process) are plotted in Figure 4.16.

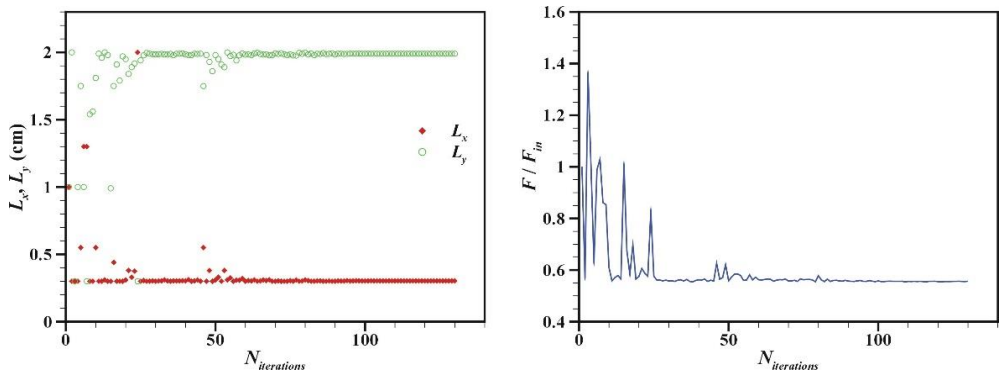

Figure 4.16-Evolution of the values of the 2 geometric parameters (left) and the relative objective function, F/F_{in} (right) during the optimization procedure for U_{in} of 0.002 m·s^{-1} (Re = 60) and w_P of 0.75.

As can be seen from Figure 4.16, 160 iterations were made, and the corresponding optimization seems to converge to geometric values of L_x = 0.303 cm and L_y = 1.990 cm, which corresponds to a relative objective function (F/F_{in}) value of 0.55. This means that the objective function reduced by 45%, proving that this optimization test is reliable, since the main goal, which was to minimize the F_{obj} was accomplished. To better visualize the effect of optimization in the system performance, the steady-state concentration, temperature, and pressure fields obtained for the initial geometry versus the final optimized structure are shown in Figure 4.17.

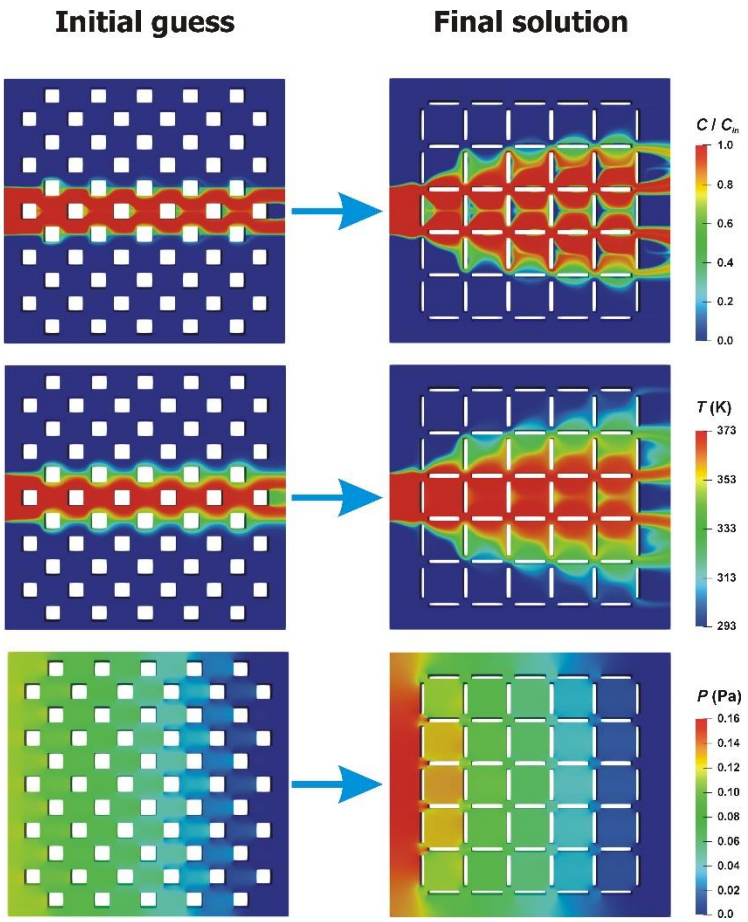

Figure 4.17-Dimensionless concentration (up), temperature (middle) and pressure (down) fields for the initial estimation (L_x = 1.0 cm and L_y = 1.0 cm) and the optimal solution (L_x = 0.303 cm and L_y = 1.990 cm). The results were obtained for U_{in} of 0.002 m·s^{-1} (Re = 60) and a w_P of 0.75.

The observation of the images in Figure 4.17 allow to conclude that the final values of the 2 optimized parameters define a geometry that enhances the level of mixing. According to what was already described in the 2D simulations section, having a higher thermal diffusivity (when compared with the mass counterpart) has a detectable effect on dispersion, which becomes even more visible in the optimized geometry. As for pressure drop, its value increased from 0.12 Pa (for the initial guess scenario) to 0.16 Pa (in the final solution), which means that this variable was not minimized. It may suggest that the weights assigned to the F_{obj} in this first test are favoring more the terms regarding dispersion/mixing. So, in a second optimization test, and for the same inlet velocity condition of U_{in} = 0.002 m·s^{-1}, the value of $\boldsymbol{w_P}$ was increased to 50 to give more relevance to the pressure drop term in the objective function. The main results obtained for the referred optimization test are plotted in Figure 4.18.

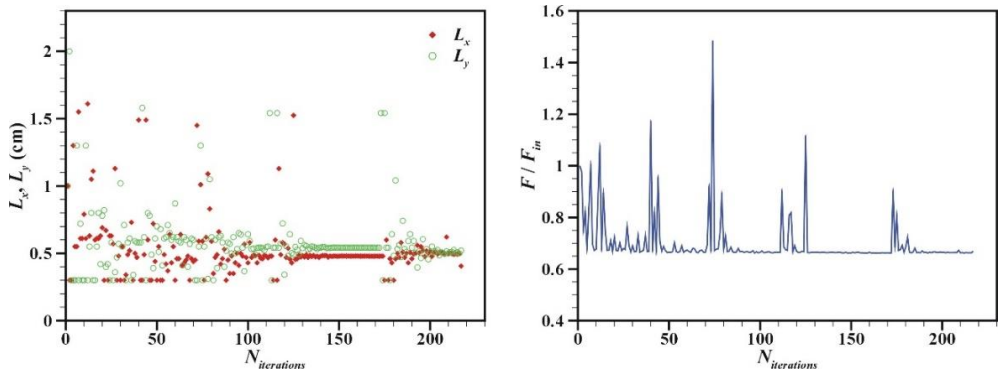

Figure 4.18- Evolution of the values of the 2 geometric parameters (left) and the relative objective function, F/F_{in} (right) during the optimization procedure U_{in} of 0.002 m·s^{-1} (Re = 60) and w_P of 50.

The optimization was stopped at around 220 iterations and the best results were assumed to be L_x = 0.498 cm and L_y = 0.510 cm (left plot of Figure 4.18). These parameters correspond to a relative objective function value of 0.66 (right plot of Figure 4.18). The convergence was not so fast and smooth than the one of the first test and, but the presented results are acceptable. Figure 4.19 shows the fields obtained for the initial guess geometry versus the final optimized structure (U_{in} = 0.002 m·s^{-1} and w_P = 50).

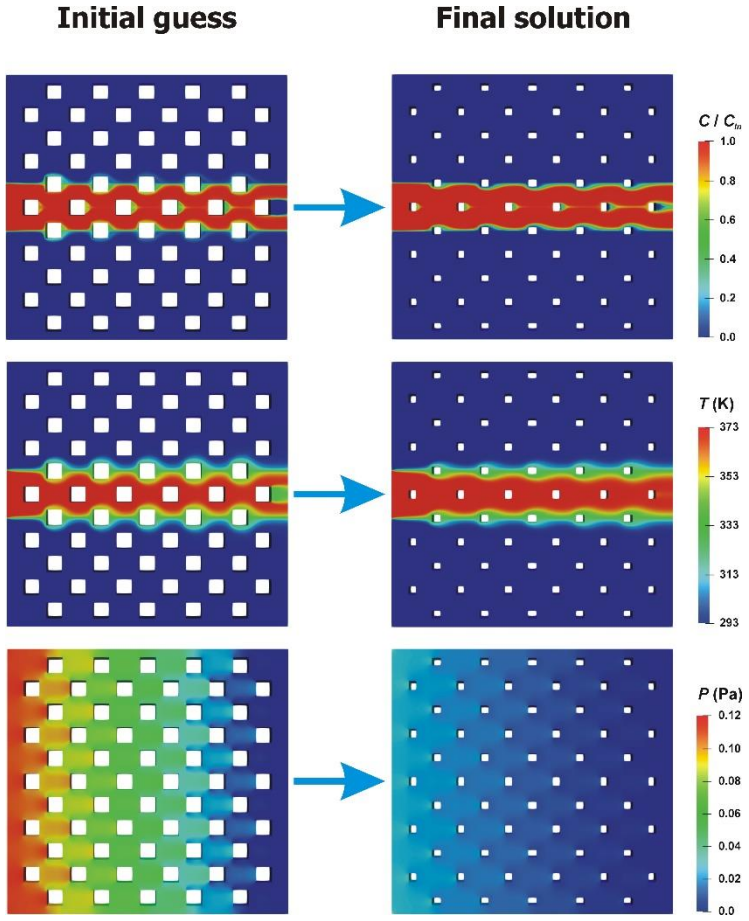

Figure 4.19- Dimensionless concentration (up), temperature (middle) and pressure (down) fields for the initial estimation (L_x = 1.0 cm and L_y = 1.0 cm) and the optimal solution (L_x = 0.498 cm and L_y = 0.510 cm) for U_{in} of 0.002 m·s^{-1} (Re = 60) and w_P of 50.

As visible in the images of Figure 4.19, the increase in the value w_P led to a geometry that provides no mixing and significantly decreases the surface area. However, as expected, the optimization was more

focused on the pressure drop term that decreased by a factor of 4 (from 0.12 Pa to about 0.03 Pa). On the other hand, as mentioned above, the mass and heat dispersion remained poor in post-optimization. So, this low velocity scenario combined with predominance of the pressure drop term (with a w_P of 50), is not appropriate to achieve good levels of mixing.

The next step was to address a higher velocity condition (U_{in} = 0.01 m·s^{-1}) in the optimization tests. However, according to the observations made in section **4.1.2 Inlet velocity effect**, the flow instabilities identified with this inlet velocity can provide a much more complex scenario to optimize. So, an optimization test with 2 geometric parameters and a w_P of 0.75 was performed, whose results obtained are plotted in Figure 4.20.

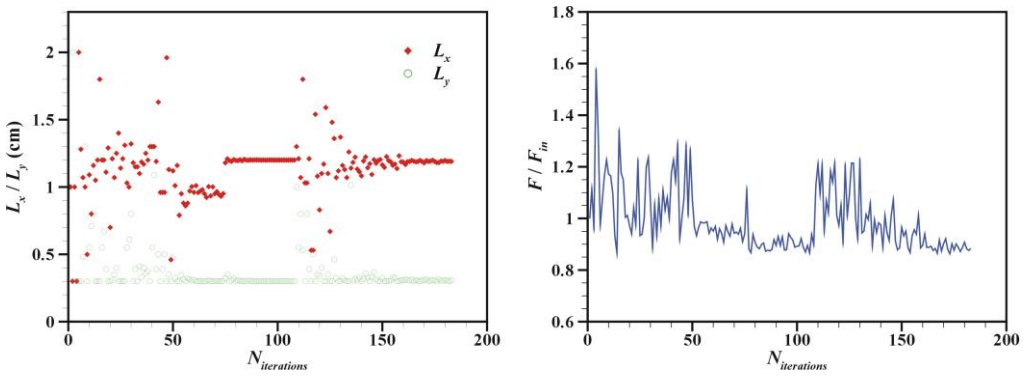

Figure 4.20-Evolution of the values of the 2 geometric parameters (left) and the relative objective function, F/F_{in} (right) during the optimization procedure for U_{in} of 0.01 m·s^{-1} (Re = 300) and w_P of 0.75.

As can be seen from Figure 4.20, the optimization is struggling to achieve a well-defined convergence and it does not seem to be successful. As such, for this velocity, it is possible that with the weights used in the F_{obj} define a function that is equally sensitive to different terms (dispersion, pressure drop and/or surface area). Coupling this possibility with the flow instabilities already pointed out for this velocity, it is created a scenario that needs further and deeper inspection in the future. Consequently, in the next optimization test for the velocity of 0.01 m·s^{-1}, it was applied a w_P value large enough to led to a predominance of the one of the terms (in this case, the pressure drop term). Since with a higher velocity, it is expected to obtain larger pressure drops, the weight factor w_P was set to a value of 15 (below the value of 50 used for a lower velocity). The main results obtained in this optimization test are plotted in Figure 4.21.

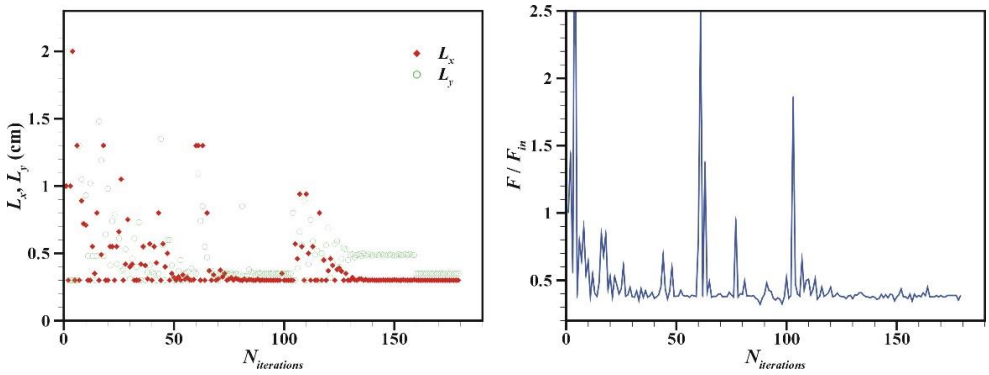

Figure 4.21- Evolution of the values of the 2 geometric parameters (left) and the relative objective function, F/F_{in} (right) during the optimization procedure for U_{in} of 0.01 m·s-1 (Re = 300) and w_P of 15.

The optimization results of the two variable geometrical parameters were assumed to be L_x = 0.307 cm and L_y = 0.350 cm (left plot in Figure 4.21), which corresponds to a relative objective function value of 0.32 (right plot in Figure 4.21). Again, the plots in Figure 4.21 suggest that more iterations would be advisable. Additionally, it is also visible some sort of "noise" in the relative objective function curve where it should be (ideally) a smooth baseline. This may be an indication of perturbances in the numerical post-treatment caused by the previously mentioned flow instabilities. Nonetheless, in Figure 4.22 are presented the fields of the initial estimate versus the final optimized structure, with U_{in} = 0.01 m·s^{-1} and w_P = 15.

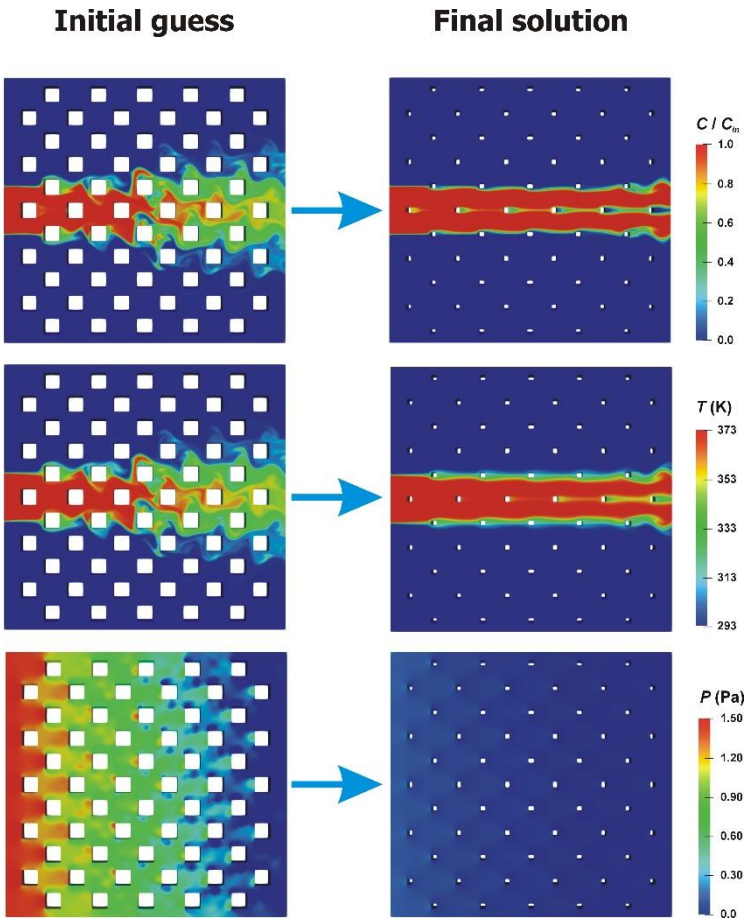

Figure 4.22- Dimensionless concentration (up), temperature (middle) and pressure (down) fields for the initial estimation (L_x = 1.0 cm and L_y = 1.0 cm) and the optimal solution (L_x = 0.307 cm and L_y = 0.350 cm) for U_{in} of 0.01 m·s^{-1} (Re = 300) and w_P of 15.

Figure 4.22 shows that the optimization results of the geometric parameters led to a significant decrease of the level of mixing (when compared with the initial guess geometry). Regarding the pressure field, even though the w_P value was considerably lower than 50 (the latter one used for a flow velocity of 0.002 m·s^{-1}), as intended, the minimization of the pressure drop was even more noticeable. In the pressure field of the initial guess geometry, it is observed the presence of blemishes in the coloring. These are other signs of the flow instabilities already detected for an inlet velocity of 0.01 m·s^{-1}. The weights attributed to the terms of the objective function were not adequate as it was not obtained a valuable geometry that while minimizing pressure drop maximizes mixing.

Finally, an optimization test was performed with 4 variable geometric parameters (L_x, L_y, α_1 and α_2) for the lower velocity condition (U_{in} of 0.002 m·s^{-1}). The weights in the objective functions are the ones used in the first test, i.e., with a w_P of 0.75. The results obtained for this optimization test are plotted in Figure 4.23.

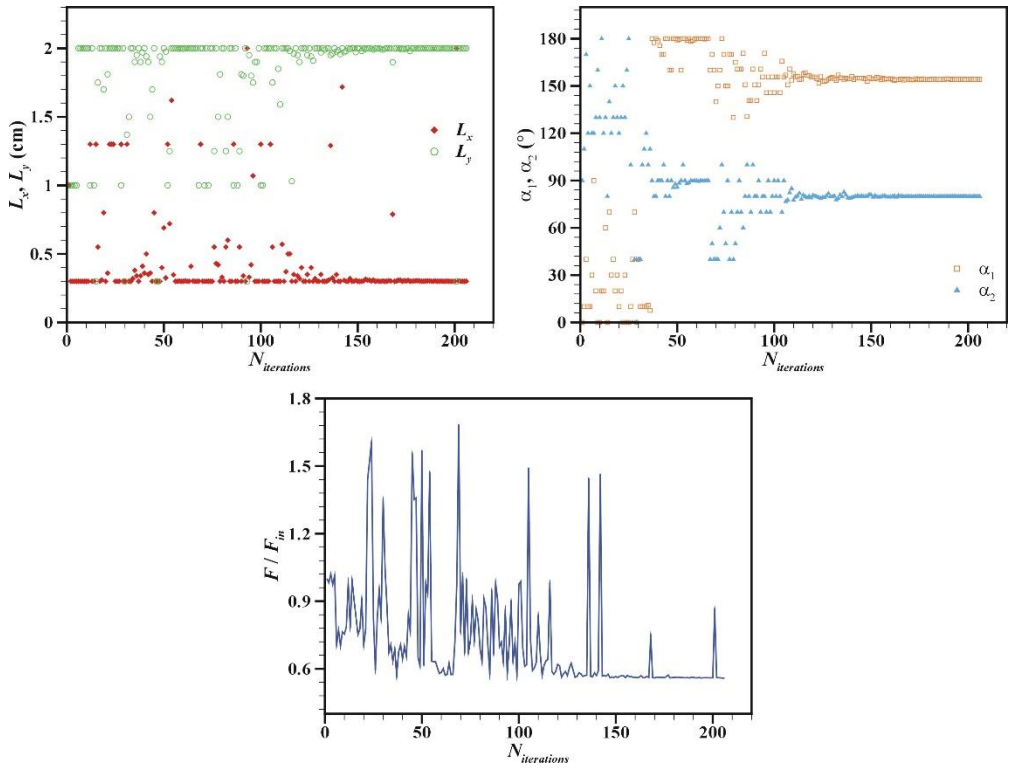

Figure 4.23- Evolution of the values of the 4 geometric parameters (upper images) and the relative objective function, F/Fin (bottom image) during the optimization procedure for U_{in} of 0.002 m·s-1 (Re = 60) and w_P of 75.

The optimization procedure was stopped at around 210 iterations and the best results obtained for the geometric values were L_x = 0.301 cm, L_y = 2.000 cm, α_1 = 154°, and α_2 = 80°. These results correspond to a relative objective function value of 0.56. From the observation of Figure 4.23, if time were available, it is clear that this optimization would improve with a deeper inspection, i.e., larger number of iterations and restart with different initial guesses due to a larger number of parameters being optimized. The fields

obtained with the initial guess geometry versus the final optimized structure are shown in Figure 4.24 (U_{in} = 0.002 m·s^{-1} and w_P = 0.75).

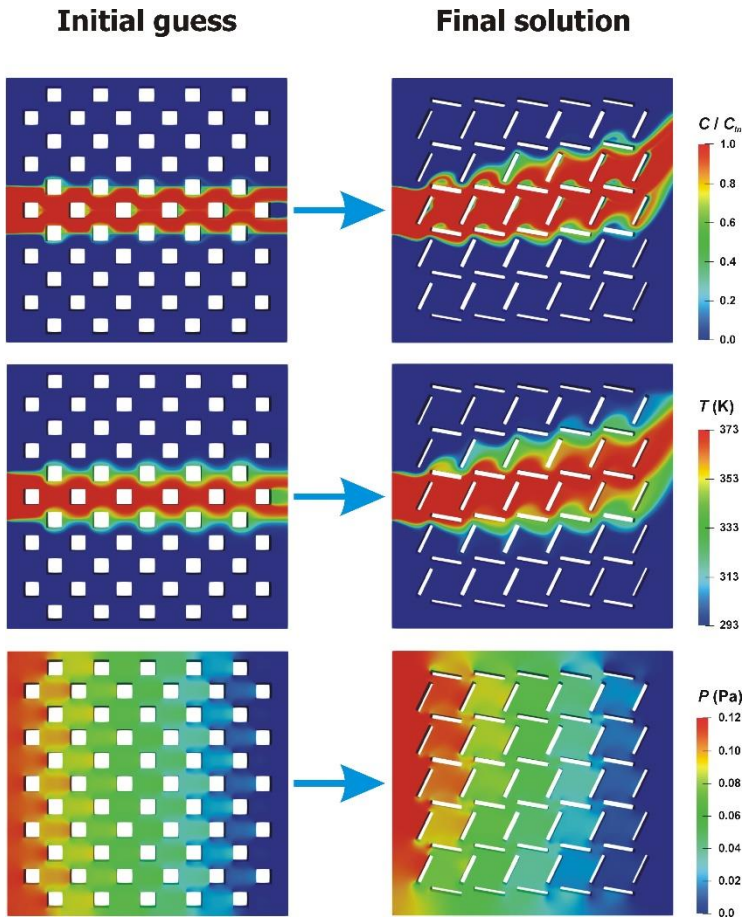

Figure 4.24- Dimensionless concentration (up), temperature (middle) and pressure (down) fields for the initial estimation (L_x = 1.0 cm, L_y = 1.0 cm, α_1 = 0°, and α_2 = 90°) and the optimal (L_x = 0.301 cm, L_y = 2.000 cm, α_1 = 154°, and α_2 = 80°) for U_{in} of 0.002 m·s^{-1} (Re = 60) and w_P of 0.75.

Based solely on the results presented in Figure 4.24, when the inclination angles are added to the set of geometric parameters to be optimized, the possible gains achieved on the mixing level are debatable. Nonetheless, when compared with the initial guess where clear preferential paths are present, it is clear that the tracer is more dispersed in the final geometry. Regarding the pressure field, again comparing with the initial guess geometry, it can be seen that the optimization did not have any effect on the pressure drop value. However, if the reference is the corresponding optimization results with 2 geometric parameters, the pressure drop has a significant reduction.

In a more in-depth study to perform in the future, it would be interesting to make optimization tests where not only the four parameters addressed are variable (L_x, L_y, α_1, and α_2), but is also allowed the obstacles to move by setting up a displacement in a defined direction. This would make up for a total of 6 geometrical parameters to optimize (one displacement value per group of obstacles). Likewise, only the weight regarding the pressure drop term in the objective function was varied in this study. The functionality of the F_{obj} intends to maximize mixing and surface area and minimize pressure drop. So,

wider studies can be performed, for different inlet velocity conditions, where the weight of the other three terms vary to assess the influence on the F_{obj}. Additionally, the functionality of F_{obj} can also be changed and adapted depending on the specificities of different applications/systems.

5 Conclusions

Within the scope of this dissertation, the single-phase flow of an incompressible Newtonian fluid coupled with mass and heat transport was simulated with computational tools, i.e., Computational Fluid Dynamics. Optimized process units are constantly sought in the area of Chemical Engineering in order to obtain a maximum efficiency, which is frequently dependent on parameters that quantify the mixture level (or dispersive phenomena) and the pressure drop. In this study, the impact of operating conditions (inlet flow velocity) and geometric parameters on the phenomena mentioned above was studied. Two sets of laminar flow simulations were carried out, in 2D and 3D geometries, addressing solid structures with ordered voids. Then, optimization tests on 2D structures were also performed.

The 2D simulations involved structures with rectangular and ellipsoidal obstacles and inlet flow velocities ranging from 0.083x10^{-2} to 1.0x10^{-2} m·s^{-1} (Re between 25 and 300). Based on the results of the mentioned simulations, it was observed a tendency for pressure drop to increase with the inlet velocity. It was concluded that the most favorable geometry in terms of pressure drop is the one with ellipsoidal voids, while regarding the mixing level, the preferable topology is the rectangular one. Based on these conclusions, the latter one (rectangular) was chosen for the subsequent optimization tests.

The 3D simulations were based on a double-tilted (45^{o}) foam structure composed by the repetition of unitary cubic cells (porosity of 0.56). The inlet flow velocities addressed on these simulations ranges from 0.010 to 0.167 m·s^{-1} (Re_{f} between 9.5 and 158.4). Regarding pressure drop, again it was confirmed the tendency to increase with the inlet velocity and, in this case, it followed the functionality of the Ergun equation. As for dispersive effects, it was observed that these are enhanced with higher velocity values and, on the other hand, the percentage of small stagnant regions decreases with U_{in}. To exemplify the set of data gathered in the 3D simulations: for the lower inlet flow velocity it was obtained D_{ax} = 8.20x10^{-6} m^2·s^{-1}, D_r = 2.63x10^{-6} m^2·s^{-1}, V_{stag} = 3.2% and , $\Delta P/L$ = 7.21x10^{2} Pa·m^{-1}; while for the higher flow velocity it was obtained D_{ax} = 1.96x10^{-4} m^2·s^{-1}, D_r = 8.84x10^{-5} m^2·s^{-1}, V_{stag} = 2.6% and , $\Delta P/L$ = 6.55x10^{4} Pa·m^{-1}.

In the last step of the thesis, it was possible to adjust a completely automatic optimization procedure (previously developed in-house). This procedure is based on geometrical parameters and included an objective function focused on maximizing dispersion and surface area and minimizing pressure drop. Optimization tests were conducted for 2D geometries with 2 and 4 variable geometrical parameters (obstacles dimensions and inclination angles). As an example, for the test with 4 variable parameters, the optimal solution found consisted on the values of L_x = 0.301 cm, L_y = 2.000 cm, α_1 = 154°, and α_2 = 80°. Apart from some limitations that still need improvement, it was demonstrated that the optimization procedure applied is operational and has the potential to be adapted to a wide range of scenarios/process units.

6 Assessment of the work done

6.1 Objectives achieved

The main objectives of this work were successfully fulfilled. A single-phase incompressible flow of a Newtonian fluid with simultaneous mass and heat transport through bi- and tridimensional porous structures was simulated and characterized. It was possible to assess the level of influence of operating variables (inlet velocity) and geometric parameters on the hydrodynamics of the studied systems. The optimization methodology was successfully implemented returning geometries with potential to enhance mixing and decrease the pressure drop.

6.2 Limitations and Future Work

The main limitation to the work developed was the short period of time foreseen for the dissertation, due to the current pandemic, which did not allow the necessary deepening of some matters, such as: experimental validation; simulations involving homogeneous chemical reaction; simulations of a two-phase flow with mass transfer; and a wider optimization testing.

Suggestions for future work in this area would be to address more complex structures, further improve and refine the optimization procedure (according to the suggestions already made) and simulate for turbulent flow. Likewise, since CFD is a complement to laboratory experiences, it would be interesting to transpose the simulated structures and conditions to the physical world, and test whether the laboratory results prove the numerical solution or not. To do this, the structures would have to be 3D printed, which should be feasible since the geometries .stl files are compatible with 3D printers and CEFT has the necessary equipment and conditions.

6.3 Final Assessment

The balance of all the work carried out was very positive, both professionally and personally. From a personal point of view, it was utterly motivating and challenging, since it encompassed various subjects from the Chemical Engineering course. Furthermore, it allowed me to go beyond the course and dive into new areas of engineering, namely coding in a new language. From a scientific point of view, it was fascinating to learn how certain phenomena may influence the performance of process units.

All in all, it was a very positive, stimulating, and fortuitous experience that further picked my interest in the vast area that is Computational Fluid Dynamics.

7 References

- Ansoni J. L., and Seleghim, P., “Optimal Industrial Reactor Design: Development of a Multiobjective Optimization Method Based on a Posteriori Performance Parameters Calculated from CFD Flow Solutions”, Advances in Engineering Software, 22-35, 2016.
- Barbosa J. C. B., “Hidrodinâmica em sistemas com estruturas do tipo open-cell foam: estudos com ferramentas de CFD”, Master thesis, Faculty of Engineering of the University of Porto, 2019.
- Baser S.A., and D.V. Khakhar D.V., “Modeling of the dynamics of R-11 blown polyurethane foam formation”, Polymer Engineering Science, **34**, 632-641, 1994.
- Bayat M., Aminian J., Bazmi M., Shahhosseini S., and Sharifi K., “CFD modeling of fouling in crude oil pre-heaters”, Energy Conversion and Management, **64**, 344-350, 2012.
- Campos J.B.M.L., “Notas para o estudo da Mecânica de Fluidos”, FEUP edições, 2013.
- Courant R., Friedrichs K., and Lewy H., "Über die partiellen Differenzengleichungen der mathematischen Physik", Mathematische Annalen, **1**, 32–74, 1928.
- Danckwerts P. V., “Continuous flow systems”, Chemical Engineering Science, **2**, 1-13, 1953.
- Delgado J. M. Q., “A critical review of dispersion in packed beds”, Heat Mass Transfer, **42**, 279-310, 2005.
- Ergun S., "Fluid flow through packed columns." Chemical Engineering Progress, **48**, 1952.
- Fogler H.S., “Elements of Chemical Reaction Engineering”, Models for Nonideal Reactors, 18, 9-23, 1986.
- Guedes de Carvalho J.R.F., and Delgado J.M.P.Q., “Mass transfer from a large sphere buried in a packed bed along which liquid flows”, Chemical Engineering Science, **54**, 1121-1129, 1999.
- Hajilary N., and Rezakazemi M., “CFD Modeling of CO2 Capture by Water-based Nanofluids Using Hollow Fiber Membrane Contactor”, International Journal of Greenhouse Gas Control, 2018.
- Hiby J. W., and Schummer P., “Zur Messung der Transversalen Effektiven Diffusion in durchstromten Fullkorpersaulen”, Chemical Engineering Science, **13**, 69-74, 1960.
- Levenspiel O., “Chemical Reaction Engineering”, John Wiley & Sons, New York, 290-293, 1972.
- Pinto A. M. R., Oliveira V. B., and Falcão D. S., “Status and research trends of direct alcohol fuel cell technology”, Direct Alcohol Fuel Cells for Portable Applications, **10**, 307-329, 2018.
- Rao, C.S., and Barik K, “Modeling, simulation and control of middle vessel batch distillation column”, Procedia Engineering, **38**, 2383-2397, 2012.
- Sourav S., Singh K. K., and Shenoy K.T., “Axial Dispersion and Pressure Drop for Single-phase Flow in Annular Pulsed Disc and Doughnut Columns: A CFD Study”, Progress in Nuclear Energy, **106**, 335-344, 2018.

- Sousa P., Soares A., Monteiro E., and Rouboa A., "A CFD Study of the Hydrodynamics in a Desalination Membrane Filled with Spacers", Desalination, 2014.
- Vuorinen V., Aarnio M., Alava M., Alopaeus V., Atanasova N., Auvinen M, et al.., "Modelling Aerosol Transport and Virus Exposure with Numerical Simulations in Relation to Sars-cov-2 Transmission by Inhalation Indoors", Safety Science, 2020.
- Advanced Simulation Library®, http://asl.org.il/.
- Autodesk®, https://www.autodesk.com/.
- COMSOL Multiphysics®, https://www.comsol.com/.
- Fluent®, https://www.ansys.com/products/fluids/ansys-fluent.
- OpenFOAM® User Guide, The OpenFOAM Foundation, version 7, retrieved on the 23th April 2020.
- OpenFOAM®, https://openfoam.org/.
- ParaView®, https://www.paraview.org/.
- SimScale®, https://www.simscale.com/.
- SU2®, https://su2code.github.io/.

Annex A – Hiby and Schummer proposed radial inlet injection

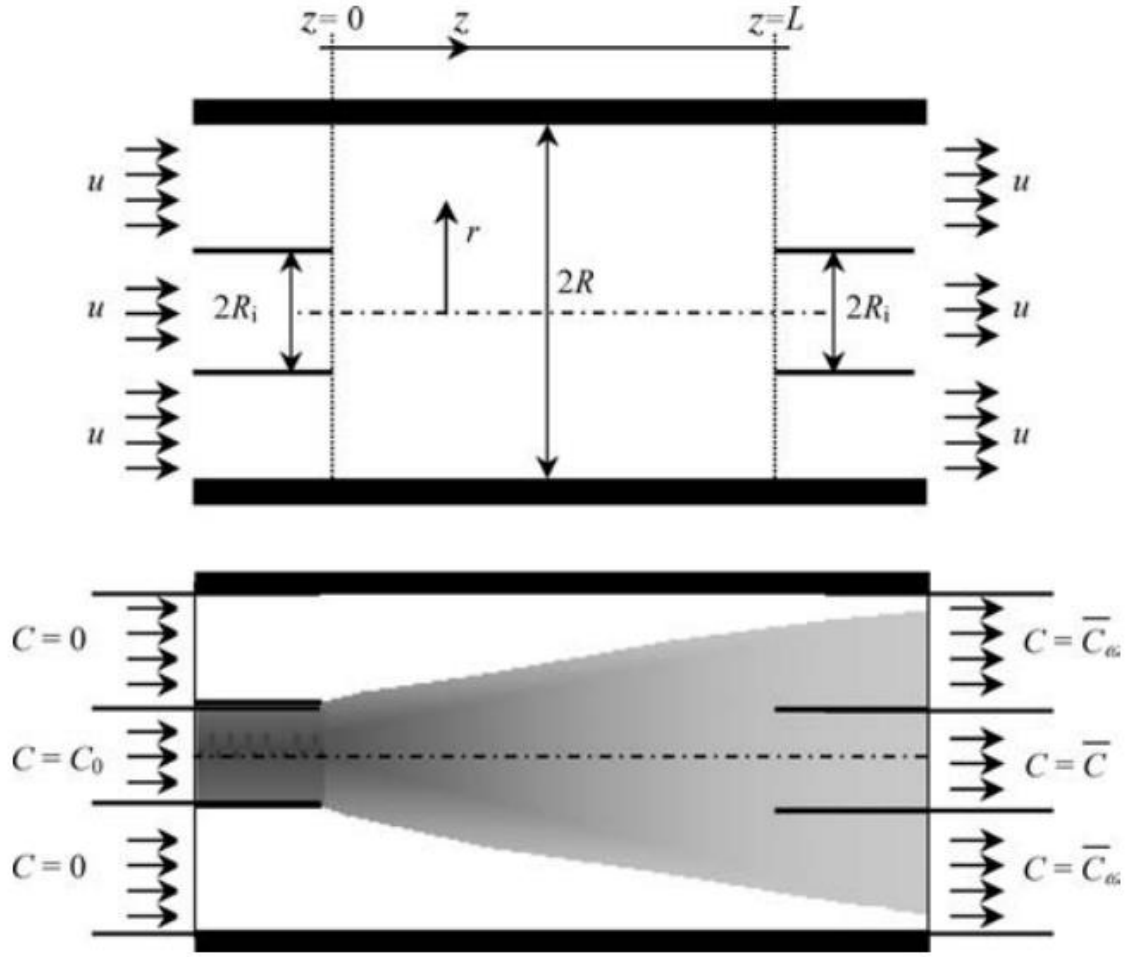

Figure A.1-Sketch of boundary conditions proposed by Hiby and Schummer (Hiby and Schummer, 1960).

References

- Hiby J. W., and Schummer P., "Zur Messung der Transversalen Effektiven Diffusion in durchstromten Fullkorpersaulen", Chemical Engineering Science, 13, 69-74 1960.

Annex B - Estimated percentage of stagnant volume versus Reynolds of the fluid, obtained for a similar geometry subjected previously to in-house studies

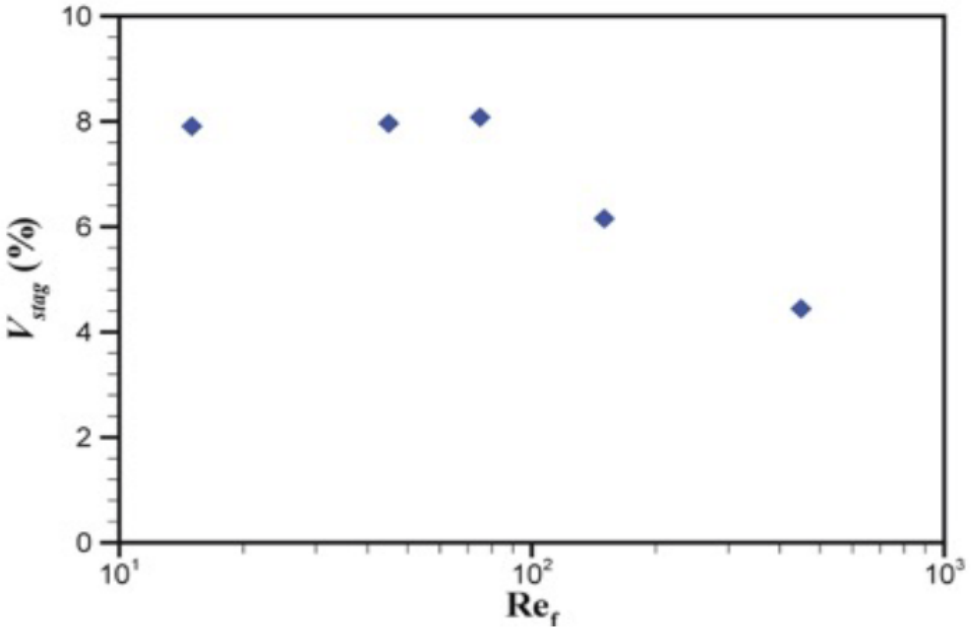

Figure A.2-Percentage of volume stagnant as a function of Re_f based on the characteristic dimension of the free distance between the struts (0.15 cm) for a 3D geometry with a length of 4cm (Barbosa, 2019).

References

- Barbosa J. C. B., "Hidrodinâmica em sistemas com estruturas do tipo open-cell foam: estudos com ferramentas de CFD", Master thesis, Faculty of Engineering of the University of Porto, 2019.

Appendix A – Initiation: Installation of needed software packages

The first step in the execution of this thesis was the installation on my personal computer of a virtual machine, the free and open-source Ubuntu, based on Linux. Then, it came the installation of OpenFOAM®, made by command line (as is normal in operating systems based on Linux). The installation package included the graphical visualization tool and post-processor ParaView®.

On a second phase, the geometry generator CF-MESH+® was installed, once again by a series of commands.

Appendix B - Learning the general functioning of the CFD software

Then it came the time to learn how to use the OpenFOAM® software. For this, I used the user manual provided by the OpenFOAM® Foundation and tutorials that already exist on various websites, from community forums to videos present on content sharing platforms such as YouTube. This step involved learning not only the basics of Linux commands and the C ++ coding language, as well as CFD concepts such as the influence of the time step on the Courant number in transient state simulations. A subset list of the videos (tutorials) followed can be seen below:

- Nagy J., "Introduction to CFD", YouTube, (2014), https://www.youtube.com/watch?v=mGSUIXye9j4.
- Nagy J., "How to run your first simulation in OpenFOAM®", YouTube, (2014), https://www.youtube.com/watch?v=KznljrgWSvo.
- Nagy J., "How to open OpenFOAM® results in ParaView®", YouTube, (2014), https://www.youtube.com/watch?v=8J59CpaYnVc&t=310s.
- Fluid Mechanics 101, "[CFD] The Courant (CFL) Number", YouTube, (2020), https://www.youtube.com/watch?v=WBWY46ynRk0.
- Nagy J., "How to create a grid with blockMesh in OpenFOAM®", YouTube, (2014), https://www.youtube.com/watch?v=Ds0eK1wXMks&t=17s.
- Nagy J., "Understanding grid convergence", YouTube, (2014), https://www.youtube.com/watch?v=lrGO9QSBq1g&t=988s.
- Nagy J., "Introduction to transport equations", YouTube, (2014), https://www.youtube.com/watch?v=PaDDplpAJJ0&t=254s.

- Nagy J., "Introduction to discretization", YouTube, (2014), https://www.youtube.com/watch?v=YTcMTuxNhoE.
- Nagy J., "How to run your first OpenFOAM® case yourself", YouTube, (2014), https://www.youtube.com/watch?v=jfDzFPaPPug&t=224s.
- Nagy J., "Introduction to stationary turbulence modeling (RAS)", YouTube, (2014), https://www.youtube.com/watch?v=IPExwi2Ar-g.
- Nagy J., "Introduction to transient turbulence modeling (RAS,LES)", YouTube, (2014), https://www.youtube.com/watch?v=l8jDBPN4rXo.
- Fluid Mechanics 101, "[CFD] The k - epsilon Turbulence Model", YouTube, (2019), https://www.youtube.com/watch?v=fOB91zQ7HJU.

Due to the pandemic and consequential confinement, I did a more in-depth learning than what would be necessary for the execution of this dissertation, as can be seen from the list above, learning concepts such as simulation of a compressible fluid and how to simulate turbulent flow (RAS and LES models).

One of the most valuable learnings was the importance of discretisation. When upon a continuum problem, discretisation is in order so that a continuum solution can be converted into discrete quantities. The purpose of discretisation is to transform the governing equations into a corresponding system of algebraic equations. Considering the generic form of the standard transport equation for any tensorial quantity $\boldsymbol{\phi}$:

$$\underbrace{\frac{\partial \rho \phi}{\partial t}}_{\text{time derivative}} + \underbrace{\nabla \cdot (\rho \boldsymbol{U} \phi)}_{\text{convection term}} = \underbrace{\nabla \cdot (D \nabla \phi)}_{\text{diffusion term}} + \underbrace{S_\phi(\phi)}_{\text{source term}} \tag{a.1}$$

where ρ is the density, $\boldsymbol{U}$ is the velocity and D the diffusivity. The terms from left to right represent the rate of change per unit volume (time derivative), the efflux by convection per unit volume (convection term), the rate of transport due to diffusion (diffusion term) and the rate of production/destruction per unit volume (source term). The tensorial quantity ($\boldsymbol{\phi}$) can be concentration ($\boldsymbol{C}$) or/and temperature ($\boldsymbol{T}$).

A finite volume discretisation of equation (a.2) is formulated by integrating over the control volume V_P and time:

$$\int_t^{t+\Delta t} \left[\int_{V_P} \frac{\partial \rho \phi}{\partial t} dV + \int_{V_P} \nabla \cdot (\rho \boldsymbol{U} \phi) dV \right] dt = \int_t^{t+\Delta t} \left[\int_{V_P} \nabla \cdot (D \nabla \phi) dV + \int_{V_P} S_\phi(\phi) dV \right] dt \tag{a.2}$$

In transient simulation a time integration is also made over the time step Δt.

Resorting to the Gauss theorem, that states that a volume integral over a divergence of a given region around the surface is equal to the external flux that goes through a closed surface, the convection and the diffusion terms can be rewritten as:

Convection term: $$\int_{V_P} \nabla \cdot (\rho \boldsymbol{U} \phi) dV = \oint_S d\boldsymbol{S} \cdot (\rho \boldsymbol{U} \phi) \approx \sum_f \boldsymbol{S} \cdot (\rho \boldsymbol{U})_f \phi_f \quad \text{(a.3)}$$

Diffusion term: $$\int_{V_P} \nabla \cdot (D \nabla \phi) dV = \oint_S d\boldsymbol{S} \cdot (D \nabla \phi) \approx \sum_f (\boldsymbol{S} \cdot \nabla \phi_f) D_f \quad \text{(a.4)}$$

where $d\boldsymbol{S}$ is the outward pointing differential of the surface area vector.

This is known as the finite volume method, when volume integrals in a partial differential equation that contain a divergence term are converted to surface integrals. These terms are then evaluated as fluxes at the surfaces of each finite volume.

Regarding the convection term, the discretization of the value ϕ_f can be made in a variety of ways. Some of the available divergence schemes are:

- Upwind
- Linear
- Linear Upwind
- Quadratic Upstream Interpolation for Convective Kinematics (QUICK)
- Cubic
- van Leer

For the purpose of this thesis, the discretization schemes used were the Linear Upwind and the van Leer.

Appendix C – Scalar Transport

Upon not discovering tutorials that approached mass transfer, a skill that I require to learn for the execution of this dissertation, I set myself to incorporate the mass transport equation into a pre-existing OpenFOAM® solver. A solver is an executable that runs the simulation and results from the compilation of: 1) a programmed file in C++ language, with extension ".c", the source code, where the actual functionality is implemented i.e. the function body; 2) the so-called header files with extension ".h", which is where the names of program elements such as variables, functions, classes, and so are declared, i.e., where it is tell how to call the functionality. Some solvers may also have additional ".c" and ".h" files that translate, for example, system boundary conditions, the flow inlet position and respective dimensions.

The adaptation was firstly made from the `scalarTransportFoam` solver because it is a simple solver, that does not simulate the fluid flow, i.e. the vectorial velocity field and the pressure field are no computed, and it was the used solver on some of the tutorials previously followed (referred in Appendix 2), so it was a familiar code. The temperature transport was already included in the solver, so coding the mass transport was done considering that both concentration and temperature are scalar variables and Fick's second law for mass has the same mathematical form as the Heat equation for temperature.

Considering that the source code of the solver was being altered, how to compile a solver was a mandatory learning. As is the case with Linux operating systems, the compilation of these files take place using the command line.

On a second phase, since `scalarTransportFoam` has the mentioned limitations, the scalar transport adaptation had to be made on a more appropriate solver, one that could simulate the fluid flow, i.e. that computes the vectorial velocity field and the pressure field. This led to choosing `pimpleFoam`, from which the mass and heat transport were incorporated as described in chapter 3.2.1 Mathematical model.

Appendix D – Historical context

Historically, one of the earliest type of calculations resembling modern CFD are those by L. F. Richardson in the 1910s. He developed the first numerical weather prediction system when dividing physical space into grid cells and using finite differences (Richardson, 1922). The calculations failed, which led to what he called the "forecast-factory". The idea was to fill a vast stadium with 64 000 people, each one equipped with calculating machines performing part of the flow calculation. A leader in the center, using colored signal lights and telegraph communication, would coordinate the forecast. What Richardson was proposing would have been a very rudimentary CFD calculation, where he would have got discrete numbers for flow from each person (each person being a cell).

In 1933, the first numerical solution of the flow field inside a two-dimensional cylinder was obtained by A. Thom (Thom, 1933). A similar solution was reached twenty years later through means of a mechanical calculator, proving the reliability of the numerical results produced years prior (Kawaguti, 1953).

The evolution of computer power throughout the 1940s paced the birth and development of CFD technologies.

The invention of CFD per se can be pinpointed to 1944 in Los Alamos National Laboratory (USA). Hans Bethe and Richard Feynman, two Noble Prize winners in physics, led the development of the finite difference method (FDM), a numerical technique for solving differential equations by approximating derivatives with finite differences, based on a one-dimensional, Lagrangian, and inviscid flow approach,. Feynman was behind the transition of human computers through mechanical calculators to IBM machines, while Bethe led the “physics” department. The finite differences failed until 1948 when J. VonNeumann and R.D. Richtmyer invented artificial viscosity (Von Neumann and Richtmyer,1948).

In the 1960s, pioneering simulations in terms of primitive variables (velocity components and pressure) were performed by a group led by F. H. Harlow. These made use of computers to model fluid flow governed by the Navier-Stokes equations. With Harlow at the helm, a variety of transient two-dimensional fluid flows algorithms were developed, most prominently Particle-In-Cell (PIC), Marker-and-Cell (MAC), Vorticity-Stream function methods, and the foundation for what has become the k-ε turbulence model. Harlow’s efforts formed the basis of engineering CFD: in 1965, his article in Scientific American with J. Fromm, showing the power of CFD experiments had such an impact, that went on to inspire an entire generation who created CFD as a force (Harlow and Fromm, 1965).

On pair with Harlow is P. Lax, who, on the awake of artificial viscosity, laid the basis for the analytical and numerical solution of hyperbolic partial differential equations (Lax, 1986). At the time, he also worked at Los Alamos National Laboratory, but even after leaving, he went on to be a prolific inventor and writer of CFD knowledge.

The term “Computational Fluid Dynamics” only came into place in 1964 when coined by C.K. Chu (Chu, 1964). Around this time, it was published the first paper (Hess and Smith, 1964) about a method for calculating the incompressible flow around three-dimensional bodies with the aid of a computer. The method consisted of a discretization of the surface of the geometry into small quadrilaterals, the designated panels. Over time, various codes using panels emerged with emphasis to the VSAERO and the USAERO. The first of which has been widely used in the development of submarines, surface ships, automobiles, helicopters, aircraft, and more recently wind turbines, while the later has been used for modelling high speed trains and racing yachts.

In the 1970s, a group working at the Imperial College (UK), under the supervision of D. B. Spalding, were prolific developers of CFD techniques, most prominently: the SIMPLE algorithm, a popular iterative numerical solver of Navier-Stokes equations; progress of turbulence simulation, with the development of the form of the k-ε turbulence model that is used today; and discretization schemes, with the development of upwind differencing. Another key event to the CFD industry dates to 1980 when S. V. Patankar published "Numerical Heat Transfer and Fluid Flow", probably the most influential book on CFD that led to the creation of innumerous new codes (Patankar, 1980).

In the early 1980s, commercial CFD codes came into the open marketplace. Instead of being limited to an exclusive number of laboratories, mainly in the aerospace sector, major companies around the world started to adopt CFD software as a valid and competitive method of testing their products or services. CFD is now recognized to be a part of the computer-aided engineering (CAE) spectrum of tools used extensively in all industries, and its approach to modelling fluid flow phenomena allows engineers to have the power of a wind tunnel testing facilities on a desktop computer. Nowadays, CFD is both used at an academic research level and at cutting edge companies to either create new products or solutions, or to enhance properties of already existing products and processes.

Interestingly enough, OpenFOAM® was created by a Chemical Engineer. Doctor Henry Weller is the culprit behind Open FOAM®, who in 1989, while at Imperial College London, wanted to develop a more capable and flexible simulation platform than the standard of the time, which used the Fortran language. This led to the choice of C ++ as a programming language, due to its modularity and object-oriented characteristics. However, what it started to be named FOAM was formerly commercially licensed, having only become open source on the 10th December 2004. The decision to make the software fully open source was taken “to service the needs of CFD users in research, development and consultancy who can benefit greatly from perpetual free access to what is essentially a programming toolbox for CFD” (Weller, Greenshields and Janssens, 2004).

References

- Chu, C. K., “Linearized hyperbolic steady magnetohydrodynamic flow past nonconducting walls”, Physics of Fluids, **7**, 707–714, (1964).
- Harlow, F. H., and Fromm, J., “Computer Experiments in Fluid Dynamics”, Scientific American, (1965).
- Kawaguti, M., “Numerical Solution of the NS Equations for the Flow Around a Circular Cylinder at Reynolds Number 40”, Journal of the Physical Society of Japan, **8**, 747-757, (1953).
- Lax, P. D., “On dispersive difference schemes”, Physica D: Nonlinear Phenomena, **18**, 250-254, (1986).
- Hess, J. L., and Smith, A.M.O., “Calculation of nonlifting potential flow about arbitrary three-dimensional bodies”, Journal of Ship Research, **8**, 22-44, (1964).
- Patankar, S. V., “Numerical Heat Transfer and Fluid Flow”, U.S.: Hemisphere Pub., (1980).
- Richardson, L. F., “Weather Prediction by Numerical Process”, Cambridge University Press, **66**, (1922).
- Thom, A., “The Flow Past Circular Cylinders at Low Speeds”, Royal Society, London, 651-666, (1933).
- Von Neumann J., and Richtmyer R. D., “A method for the numerical calculation of hydrodynamic shocks”, Journal of Applied Physics, **21**, 232–237, (1950).
- Weller, H., Greenshields, C. and Janssens M., “OpenFOAM 1.0 Released”, The OpenFOAM Foundation, (2004).

Appendix E - *F*(t) curve obtained numerically and theoretically adjusted

The numerical $F(t)$ curve is given by:

$$F(t) = \frac{C_{out}(t)}{C_{in}} \tag{2.10}$$

Yet, it was observed that the system has dispersive effects, which can be accounted for in the $F(t)$ curve by fitting to the following equation (piston-type with dispersion model):

$$F(t) = \frac{1}{2}\left[1 - \text{erf}\left(\frac{L - u_{int}t}{2\sqrt{D_{ax}t}}\right)\right] \tag{3.2}$$

Furthermore, it was detected that the system has stagnant zones, which can be estimated by adding the a time shift (parameter t_{stag}) to Equation 4.1:

$$F(t) = \frac{1}{2}\left[1 - \text{erf}\left(\frac{L - u_{int}(t + t_{stag})}{2\sqrt{D_{ax}(t + t_{stag})}}\right)\right] \tag{4.1}$$

Figure A.3 shows the plotted $F(t)$ following the three Equations above (simulation, equation 3.2 and equation 4.1) for the 3D geometry when the inlet velocity is 0.10 m·s^{-1} (Re = 95.0).

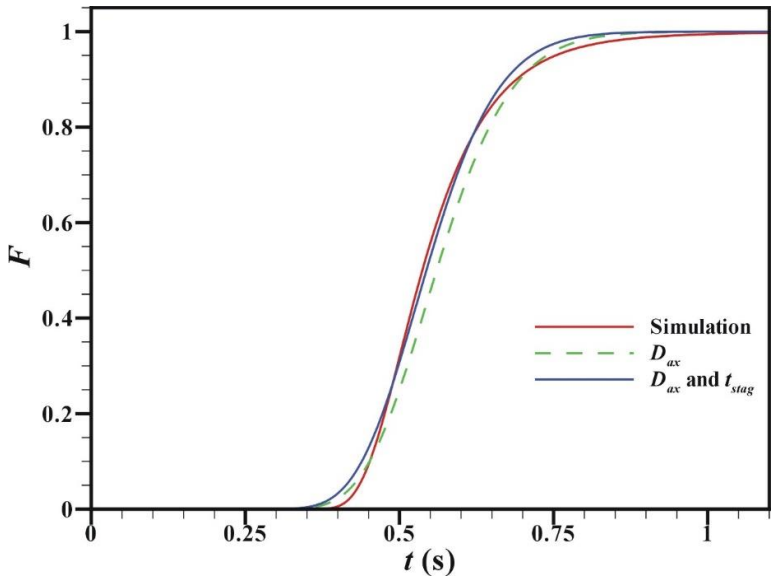

Figure A.3-Representation of the *F*(*t*) curve obtained numerically, adjusted with one parameter (axial dispersion) and adjusted with two parameters (axial dispersion and stagnant time).

In the Figure A.3, it can be seen that the equation with two fitting parameters describes better the simulation results of the outlet dimensionless concentration profile. This confirms that the system does presents axial dispersion and stagnant regions. The values obtained for the two parameters are: D_{ax} = 1.19x10^{-5} m^2·s^{-1} and a t_{stag} that corresponds to a stagnant volume ($V_{stag} = (t_{stag}/\tau)$x100) of about 2.8% of the total volume of the structure.